Open questions on toxic heavy metals Cd, Hg and Pb binding small components of DNA and nucleobases. Are there any predictable trends?

Álvaro Pérez-Barcia, M. Merced Montero-Campillo, Al Mokhtar Lamsabhi, Jean-Yves Salpin, Manuel Yáñez

Open questions on toxic heavy metals Cd, Hg and Pb binding small components of DNA and nucleobases. Are there any predictable trends?

Álvaro Pérez-Barcia[1], M. Merced Montero-Campillo[2], Al Mokhtar Lamsabhi[2], Jean-Yves Salpin*,[3,4] Manuel Yáñez*[2]

1 Departamento de Química Física, Universidad de Vigo, Lagoas-Marcosende s/n, 36310 Vigo, Spain
2 Departamento de Química, Módulo 13, Facultad de Ciencias, and Institute of Advanced Chemical Sciences (IAdChem), Universidad Autónoma de Madrid, Campus de Excelencia UAM-CSIC, Cantoblanco, 28049 Madrid, Spain
3 Université Paris-Saclay, Univ Evry, CNRS, LAMBE, 91025, Evry-Courcouronnes, France
4 LAMBE, CY Cergy Paris Université, CNRS, 95000 Cergy, France

*manuel.yanez@uam.es, jeanyves.salpin@univ-evry.fr

Abstract

In this perspective article, we provide a bibliographic compilation of experimental and theoretical work on Cd, Hg, and Pb, and analyze in detail the bonding of M^{2+} and CH_3M^+ (M= Zn, Cd, Hg, Pb) with urea and thiourea as suitable models for larger biochemical bases. Through the use of DFT calculations, we have found that although in principle binding energies decrease according to ionic size (Zn^{2+} > Cd^{2+} > Pb^{2+}), Hg^{2+} largely breaks the trend. Through the use of EDA (Energy Decomposition Analysis) it is possible to explain this behavior, which is essentially due to the strong contribution of polarization to the binding. This conclusion is ratified by the NEDA (Natural Energy Decomposition Analysis) formalism, showing that the charge transfer term is very large in all cases, but particularly in the case of the mercury-thiourea system. The general trends observed for the interactions with CH_3M^+ monocations show however CH_3Hg^+ binding energies systematically smaller than the CH_3Zn^+ ones, likely because the relativistic contraction of the Hg orbitals is very much attenuated by the attachment to the methyl group. Finally, we have investigated the gas-phase reactivity between $EtHg^+$ and uracil to compare it with that exhibited by CH_3Hg^+ and n-$ButHg^+$ previously described in the literature. This comparison gathers new information that highlights the importance of the length of the alkyl chain attached to the metal on the mechanisms of these reactions. For methyl mercury, only the alkyl transfer process is allowed; for butyl mercury, protonation is clearly favored, and for ethyl mercury, both paths are competitive experimentally.

Introduction

Among heavy metals, mercury, cadmium and lead have always been in the spotlight, catching the attention of biologists and chemists for their obstinacy in binding biological systems. This well-deserved stardom is associated with the long list of problems derived from their persistence and toxicity, which in the modern world is translated to an omnipresence in environmental and public health policies. Indeed, they induce neurological problems implicated even in Alzheimer's disease,[1] but can also accumulate in other vital organs.[2] Although evenly distributed in the Earth's crust, Cadmium (Cd) is classified as a rare element, as its average concentration is of ~0.05-015 mg/kg.[3-5] Anthropogenic use of Cd started during the 19th century and because of its physicochemical properties, has been used in many applications. One may mention for example its use to protect steel from corrosion, in paint industries,[6] and more recently in the production of alkaline batteries,[7] metal alloys, pigments in ceramics or as a stabilizer for plastics.[8] Two centuries of human activities have strongly perturbed the biogeochemical cycle of cadmium, and this metal is now one of the major contaminants in food (fish, vegetables)[8], drinking water[9] and it is also found in cigarettes.[10] This human exposure is of major concern as cadmium is one of the highly toxic metals, even at low concentrations. This element has been classified as carcinogenic (type I), and different studies indicate that cadmium exposure is associated with different types of cancers, such as kidneys, pancreas, lungs, testicles, or prostate.[11-13]

It seems also well stablished that, as many other transition metals, Hg binds to nucleobases.[14] Curiously however, unlike most metals, Hg has no known physiological attention as a nutrient or in any other natural function,[15] but it has always drawn particular attention because it is a major environmental contaminant. In nature, the high solubility of Hg^{2+} makes it strongly phytotoxic.[16] It is also one of the most dangerous elements for human beings, causing serious damage to the brain, as well as to other human organs.[17] It is important to emphasize that alkyl mercury monocations, in particular methyl mercury (CH_3Hg^+), are strong neurotoxicants and, what is worse, CH_3Hg^+ can be found in the environment and in the food chain.[18, 19] Its toxicity has been associated with its interaction with cysteine and selenocysteine, due to the high affinity of Hg to sulfur and selenium.[20, 21]

Lead poisoning was already present in antiquity[22, 23] and even if this metal was heavily used, its poisoning activity was neither well defined nor well characterized. Even during the 20th century, some critical questions concerning lead poisoning were not

solved, and some of them, as poisoning from lead paint or from water or food intake (mainly in cereals and vegetables),[24] are still open nowadays.[25]

An extensively annotated compilation of experimental and theoretical work on these three metals focused on their interaction with biological systems (15 pages and 156 references) is presented in the Supporting Information.

In this article, we will show the complexity of these ions through some new experimental and theoretical results that illustrate the difficulty in understanding the differences observed between them. Specifically, in the next section we will analyze our present knowledge and the opened questions related to the bonding features of systems containing these three metals. In subsequent sections, we will analyze the clusters formed by urea and thiourea when they interact with M^{2+} and CH_3M^+ (M= Zn, Cd, Hg, Pb), and the role played by the R alkyl chain in the reactivity of RHg^+ monocations with uracil as a good representative of small biochemical systems.

Bonding features of Cd, Hg and Pb containing systems.

The nature of the bonding, as well as the bonding capacity of these three toxic metals, have been and still are fundamental concepts that attract much attention. Taking into account the location of Cd and Hg in the periodic table, it is necessary to first compare the size effect along Group 12 and include Zn as well. Although it seems well established that when interacting with different organic compounds Zn, Cd and Hg are very often in their +2 oxidation state,[26-30] it seems also clear, after several studies carried out during the first decades of the 21st century, that there is a whole universe associated to complexes in which these metals are in a zero oxidation state.[31-38] The formation of compounds involving these transition metals and halogens can be easily understood through a charge transfer from the metal to the halogen atoms, due to the electronegativity of the latter.[39, 40] The analysis is not so simple, however, when other elements are involved. Particularly interesting is the bonding in mercury chalcogenides HgE (E= O, S, Se) and in HgA (A = Li, Na, K, Rb) molecules. In the first case, because Hg is a closed-shell and the HgE molecules are a weakly bound triplet in the ground state,[32] being the formation of Hg_2E_2 dimers very much favored.[32] In the second case, alkali atoms are more electropositive than Hg and no charge transfer should be expected from Hg to the alkali metal, these compounds being described as orbital-driven van der Waals complexes.[41] One of the most complete analysis of the bonding of HgX derivatives was reported in 2008 by Cremer et

al.[42], where X covers a large variety of electron-withdrawing and electron-donating functional groups. The fact that in the ground state Zn, Cd and Hg have a full ns^2 valence electron configuration, also explains why their dimers are very weakly bound.[37, 43] In this sense they behave very much as the alkaline-earth metals and in particular as Be, for which the existence of the Be_2 was the subject of controversy until the very last years of the 20th century and the beginning of this century.[44-47] This is one of the differences as far as Pb is concerned. Lead interacts very often in its +2 oxidation state as Zn, Cd and Hg do, but it is not a closed-shell in the ground state.

One of the aspects in which the bonding information concerning these three metals is very scarce is the relative strength of the bonds in which they participate. Assuming an ionic model, one can tentatively anticipate that bonding should be weaker for Pb than for the other transition metals[48], among other reasons, because of the larger size of Pb^{2+}, but it is not so obvious what the trend should be when the interactions involve the three transition metals Zn, Cd and Hg. One may naively think, using similar arguments, that the strength of the interaction should decrease as one goes down the group, the strongest binding being for Zn; but that would only apply again for purely electrostatic interactions involving point charges. The information is also scarce when the interaction involves CH_3M^+ (M = Zn, Cd, Hg), although some seminal papers for the particular case of CH_3Hg^+ have been reported. We will highlight here the one involving the interaction of CH_3Hg^+ with water,[48] and its role in the so-called Rabenstein's reactions.[49]

Hence, the main objective of the next section will be to provide a new perspective as far as the bonding peculiarities of these metals are concerned by investigating the strength of the bonding of M^{2+} and CH_3M^+ (M= Zn, Cd, Hg, Pb) when interacting with oxygen and sulfur bases. As suitable model systems, we have chosen urea and thiourea, which can be considered good representatives of larger biochemical bases, thanks to their conjugated O, N and S basic sites.

Urea and thiourea complexes with M^{2+} and CH_3M^+ (M= Zn, Cd, Hg, Pb)

To analyze the bonding in complexes between urea or thiourea with M^{2+} and CH_3M^+ (M= Zn, Cd, Hg, Pb) we have carried out B3LYP calculations using for metals Cd, Hg and Pb a DEF2-TVZPPD basis set expansion which includes a core pseudopotential to account for relativistic effects, and a 6-311+G(d,p) expansion for the remaining atoms of the system. To ensure that the B3LYP functional provides a reliable

description for these systems, we have carried out for the urea-M^{2+} global minima as suitable reference systems, new calculations by replacing the B3LYP functional by the M06-2X and ω-B97XD ones, which were specifically designed to deal with transition-metals. This comparison (see Figure S1 of the Supporting Information) shows small differences in the calculated binding energies between the three functionals, but the information obtained, as far as the relative stability of the complexes is concerned, is practically independent of the functional used. For this reason, in what follows we are going to discuss only the B3LYP results.

The M^{2+} binding energies for urea and thiourea are summarized in Table 1 and plotted in Figure S2 of the Supporting Information.

Table 1. Calculated binding energies ($kJ \cdot mol^{-1}$) between urea and thiourea with M^{2+} (M = Zn, Cd, Hg, Pb) metal dications.

	Urea	Thiourea	First empty orbital
Zn^{2+}	-719.5	-827.5	4s
Cd^{2+}	-583.3	-711.3	5s
Hg^{2+}	-681.2	-869.2	6s
Pb^{2+}	-477.5	-500.6	6p

The first conspicuous fact is that the smallest binding energy is obtained for Pb^{2+} that, as we mentioned above, is the largest dication among the four. Nevertheless, and despite the Cd^{2+} binding energies being smaller than those of Zn^{2+}, those of Hg^{2+} are clearly larger than those of Cd^{2+} and for thiourea even larger than that of Zn^{2+}. So, although in principle binding energies decrease according to ionic size ($Zn^{2+} > Cd^{2+} > Pb^{2+}$), Hg^{2+} largely breaks the trend. For the urea-M^{2+} complexes, the peculiarity showed by Hg^{2+} is also reflected in the structure of the complex. As illustrated in Figure 1, whereas the global minimum for both Zn^{2+} and Cd^{2+} corresponds to a structure in which the metal cation bridges between the two basic sites of urea, for Hg^{2+} the dication only interacts with the carbonyl group, the bridged structure being 16.4 $kJ \cdot mol^{-1}$ higher in energy. Finally, Pb^{2+} interacts only with the carbonyl group, but differently from Hg^{2+}, in a linear arrangement, which will be explained later on.

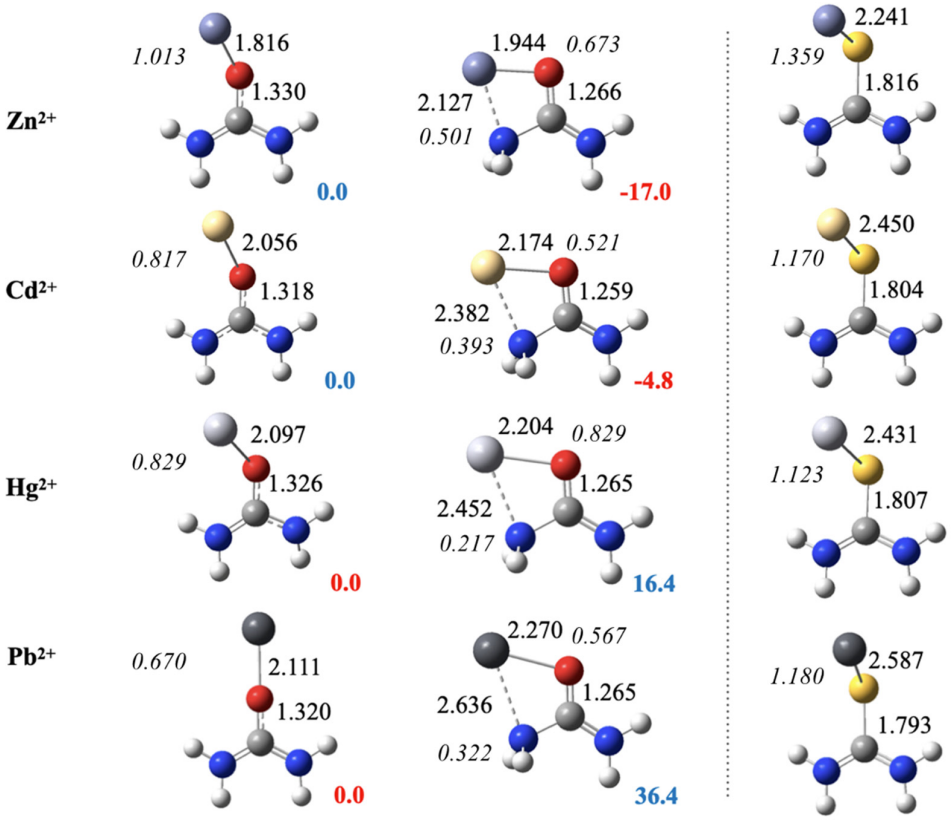

Figure 1. Structures, bond orders and relative stabilities of the unbridged (O) and bridged (N,O) conformers of urea-M^{2+} and thiourea-M^{2+} (M = Zn, Cd, Hg, Pb) complexes. Bond lengths are given in Å and relative energies in $kJ \cdot mol^{-1}$. Color code: distances in black, bond orders in italic black, energies in blue and red.

Why for Zn^{2+} and Cd^{2+} the bridged structures are favored can be understood if we examine the interactions between the two fragments, the urea and the metal dications, by means of the NEDA (Natural Energy Decomposition Analysis) method[50, 51] in the framework of the Natural Bond Orbital (NBO) method[52] shown in Figure 2. This method identifies the orbitals more involved in the interaction between the fragments and assigns an interaction energy to each overlap.

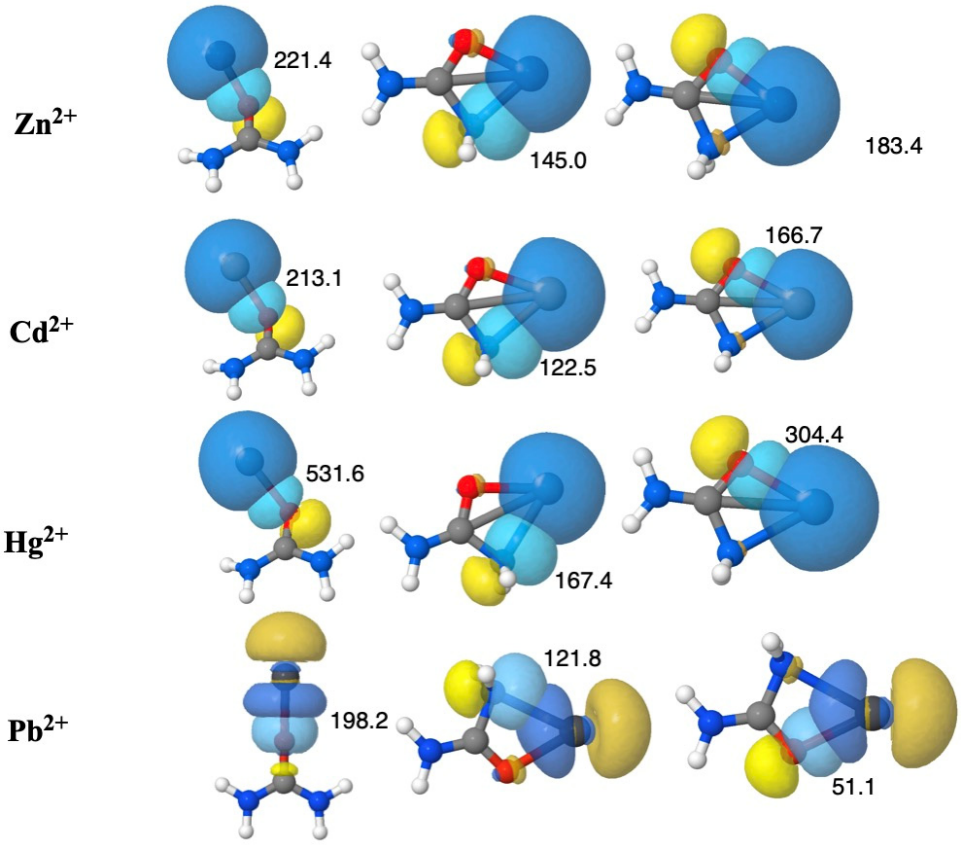

Figure 2. Interactions between the NBO localized hybrids on urea and the metal dications responsible for the monodentate complex (first column) and the bidentate one (second and third columns). Interaction energies in kJ·mol^{-1}.

In all cases there is an interaction of an occupied orbital of the base with an empty orbital of the metal dication. The first column corresponds to monodentate complexes in which the interaction involves only the lone-pair of the carbonyl group and the *ns* or *np* orbital of the ion. The second and third columns correspond to bidentate arrangements, when the charge transfer to the metal comes simultaneously from the lone-pair of one of the amino groups (second column) and from the carbonyl group (third column). It is worth noting that for Zn^{2+} and Cd^{2+} the last two interactions are more stabilizing than the interaction involving only the carbonyl lone pair, explaining why for these two metal cations the global minimum is bidentate. For Hg^{2+}, on the contrary, the interactions associated with the bridged structure are less stabilizing altogether than the interaction only with the carbonyl group, and therefore the global minimum for Hg^{2+} is monodentate. It is also evident that the interaction is much stronger when Hg^{2+} is involved, as a direct consequence of the relativistic contraction of its *6s* orbital.[53] The important quantitative

differences are also related to the charge transfer to the metal, which accounts very differently for each ion. The enhanced charge transfer in the case of Hg is nicely reflected in the net charge at the metal within the complex (+1.42), which is significantly smaller than those obtained for Zn and Cd (+1.69 and +1.68, respectively). The situation is slightly different when Pb^{2+} is involved because the charge transfer from the base goes to a *p* orbital, rather than to an *s* orbital. Since the empty *p* orbitals are degenerate, the transfer involves more than one *p* orbital, so that the electron density distribution has cylindrical symmetry along the C-O-Pb axis, leading to a linear C-O-Pb arrangement. On top of that, the interaction is much weaker than for the three transition-metal dications because of the larger size of Pb^{2+}, which is also reflected in the much higher positive charge at the metal within the complex (+1.83).

For Zn^{2+}, Cd^{2+} and Hg^{2+} the situation changes upon moving from urea to thiourea where, due to the larger volume of the sulfur lone-pair, the overlap with the empty *s* orbital of the metal dication is very effective (see Figure 3) and in all cases the monodentate complex is the global minimum. Also consistently, the interaction energies are much larger than for urea-containing complexes, since the charge transfer from the base to the metal ion is also larger as shown by the lower positive charges at the metals within the complexes (+1.33, +1.33, +1.11 for Zn, Cd and Hg, respectively). For Pb^{2+} the situation is totally similar, with a larger charge transfer than with urea (+1.53) but smaller than for the other metals.

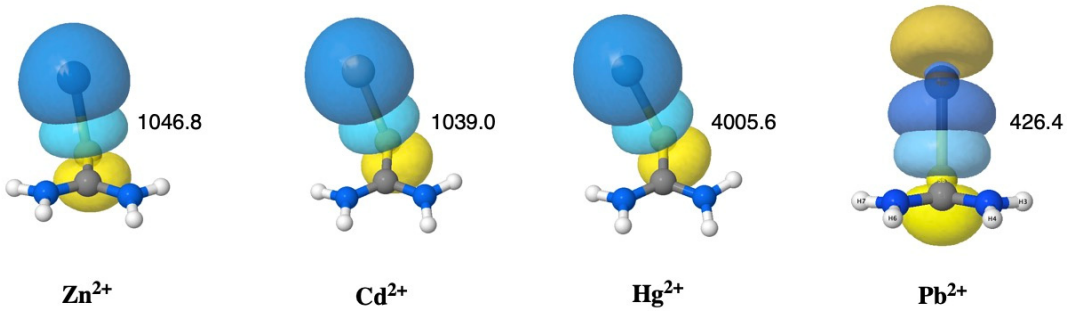

Figure 3. Interactions between the NBO localized hybrids on thiourea and the metal dications responsible for the stability of the global minima of the corresponding complexes. Interaction energies in $kJ \cdot mol^{-1}$.

So far, we have quantified the strength of the complexes and analyzed them in terms of orbital interactions, which have revealed the first reasons behind the behavior of

the series. The next step will be to analyze the systems taking into account the physical nature of the different energy contributions to the total interaction by means of the EDA (Energy Decomposition Analysis) method from Mandado's group[54], which will be confronted later on with some of the results obtained by NEDA[50, 51]. It is important to highlight that the EDA method we have used here is based on the electron density, and therefore not dependent on orbital choices.

Table 2. Interaction energy components (kJ·mol^{-1}) obtained at the B3LYP/6-311+G(d,p) (Zn^{2+} complexes) and B3LYP/DEF2-TZVP (Cd^{2+}, Hg^{2+}, Pb^{2+}) levels of theory for urea and thiourea complexes with Zn^{2+}, Cd^{2+}, Hg^{2+} and Pb^{2+}. For the urea complexes, the two binding patterns are specified by labels urea (O) and urea (O,N). Energy contributions are labeled as follows: Total (total interaction energy), Elec (electrostatic), Pauli (Pauli repulsion), Pol (polarization), Disp (dispersion), Ind (induction), Def_1 (intramolecular deformation) and Def_2 (intermolecular deformation). The ratio between polarization and electrostatic contributions (P/E) is also given.

	Total	Elec	Pauli	Pol	Disp	Ind	P/E	Def_1	Def_2
Zn^{2+}									
Urea(O)	-762.3	-573.2	275.3	-465.3	-834.7	369.4	0.81	-2104.7	1489.6
Urea(ON)	-816.3	-574.9	282.4	-524.7	-925.9	401.2	0.91	-2410.3	1783.7
Thiourea	-868.2	-445.6	235.1	-658.6	-1191.6	533.0	1.48	-3105.0	2302.5
Cd^{2+}									
Urea(O)	-631.8	-479.9	114.6	-267.4	-521.7	254.4	0.56	-1592.1	957.4
Urea(ON)	-669.4	-505.0	213.0	-377.8	-661.5	283.3	0.75	-1633.3	1074.8
Thiourea	-749.8	-417.6	184.5	-517.6	-974.5	457.3	1.24	-2554.0	1801.2
Hg^{2+}									
Urea(O)	-749.8	-526.8	252.3	-475.7	-857.3	381.6	0.90	-2232.5	1417.0
Urea(ON)	-750.6	-523.0	254.0	-482.4	-872.8	390.4	0.92	-2260.6	1470.7
Thiourea	-912.5	-489.5	256.9	-680.3	-1289.5	609.2	1.39	-3445.7	2476.4
Pb^{2+}									
Urea(O)	-522.6	-439.7	348.9	-432.2	-430.1	-2.1	0.98	-710.1	200.7
Urea(ON)	-528.4	-449.8	346.4	-425.5	-580.7	155.6	0.95	-1268.5	727.6
Thiourea	-530.9	-357.3	329.7	-503.8	-802.5	298.7	1.41	-1906.4	1268.6

Table 2 contains the different contributions to the total interaction energy obtained for the studied systems, from which the electrostatic (Elec), Pauli repulsion (Pauli) and polarization (Pol) contributions can be identified. When resourcing to second-order Raleigh-Schrödinger perturbational theory (RSPT) the latter contribution (Pol) can be further decomposed into two terms, induction and dispersion.[55] This electron density-based method does not account specifically for charge transfer contributions, which are naturally included as a part of the polarization term. Also, it is important to note that the

dispersion term is not purely dispersion as it also accounts for higher order polarization terms; nonetheless, dispersion is the dominant contribution. As it can be noticed at first glance, the total interaction energies are very high in all cases, where thiourea complexes give significantly larger values than the urea ones, as a consequence of the softer character of the sulfur basic site. The values and energy ordering are essentially in line with the previously commented binding energies. It is also known from RSPT that second order energy corrections are dependent on first order corrections to the wavefunction (or density) and, as such, induction and dispersion should not be subject to analysis as the fundamental assumption of a weak interaction has not been fulfilled. First order terms, however, are subject to interpretation and, as such, it is worth noting the relatively small contribution from the Pauli component as it reflects the bonding character of the interactions studied, with electron exchange playing here a more significant role. This observation is, in fact, in good agreement with both the large interaction energies and the interatomic distances shown in Figure 1. Indeed, the bond orders shown in Figure 1 (cursive black numbers) are larger than 1.0 for the thiourea complexes: 1.359 (Zn^{2+}), 1.170 (Cd^{2+}), 1.123 (Hg^{2+}) and 1.180 (Pb^{2+}).

Taking as a reference the ionic experimental radii (Zn^{2+}, 88 pm; Cd^{2+}, 109 pm; Hg^{2+}, 116 pm; Pb^{2+}, 133 pm)[56] it is clear that Hg^{2+} defies the expected trends. In fact, the polarization term is contributing almost as much as the electrostatic term in many cases or even much more, as revealed by the polarization/electrostatic ratio shown in Table 2. The polarization value is much larger than the electrostatic one (1.48, 1.24, 1.39, 1.41) in all thiourea complexes, whereas it is less than 1.00 or even largely below this value (0.56 for Cd^{2+}) in the urea complexes. In other words, the EDA results clearly explain why the ionic model expected trends are not valid in the series and account for the strong contribution of polarization in the binding.

As explained before, the polarization term is decomposed into induction and dispersion contributions (Table 2). It is striking, however, to find positive induction values, although the global polarization term is clearly negative. This is not an artifice of the method but has instead physical grounds on the nature of the systems, arising from the fact that the interaction is far from a closed shell intermolecular interaction; instead, a real bond is formed. This is evident when looking at the terms Def_1 (all negative) and Def_2 (all positive) in Table 2, accounting for the intramolecular and intermolecular deformation energies.[55] The very large negative values obtained for the intramolecular deformation speak for the relevance of charge transfer in complex formation as for

weakly interacting systems, where charge transfer is very small, stabilization is gained from the intermolecular deformation term, whereas the intramolecular ones are positive due to the deformation of the electron density. The outstanding values found for mercury are fully in line with a very large charge transfer in the thiourea complex.

We previously discussed the natural atomic charge on the metal upon complexation as a rough way to estimate the charge transfer, but this quantification can also be provided by NEDA. To confirm the findings of the EDA method, we have compared them to the NEDA results. Table 3 summarizes the charge transfer results compared to the total interaction energy, along with the detailed natural atomic charges values (note again that the charge exhibited by mercury in the thiourea complex, +1.116, means in practice a one-electron reduction upon complexation). Obviously, the total interaction energies are almost identical to the ones obtained with the EDA method. A linear relationship has been found between the charge transfer contribution and the natural charges with a regression coefficient of R^2=0.96. The charge transfer term is very large in all cases, but particularly in the case of the mercury-thiourea system, which is the highest one of the whole series (-903.6 kJ·mol^{-1}).

Table 3 Total interaction energy (Total, (kJ·mol^{-1})), charge transfer contribution (CT, kJ·mol^{-1}) and natural atomic charges (charge) obtained with the NEDA-NBO methods for the urea and thiourea complexes with Zn^{2+}, Cd^{2+}, Hg^{2+} and Pb^{2+}. Charge values are all positive.

	Total	CT	Charge
Zn^{2+}			
Urea(O)	-763.0	-329.3	1.705
Urea(ON)	-817.0	-383.1	1.694
Thiourea	-868.8	-709.2	1.331
Cd^{2+}			
Urea(O)	-632.3	-310.4	1.662
Urea(ON)	-670.0	-319.0	1.685
Thiourea	-750.5	-637.8	1.330
Hg^{2+}			
Urea(O)	-750.2	-557.4	1.422
Urea(ON)	-751.4	-476.1	1.518
Thiourea	-913.3	-903.6	1.116
Pb^{2+}			
Urea(O)	-523.2	-284.5	1.830
Urea(ON)	-528.7	-330.5	1.739
Thiourea	-531.4	-531.1	1.531

Once we have understood the binding of the series of dications, it is time to check what happens if we move to alkyl metal cations. To stick to the simplicity of the model, we chose for the analysis the simplest alkyl chain, methyl. The general trends when dealing with CH_3M^+(M = Zn, Cd, Hg, Pb) complexes, whose structures are shown in Figure 4, do not change significantly, though the binding energies are necessarily much smaller than those obtained for the corresponding dications.

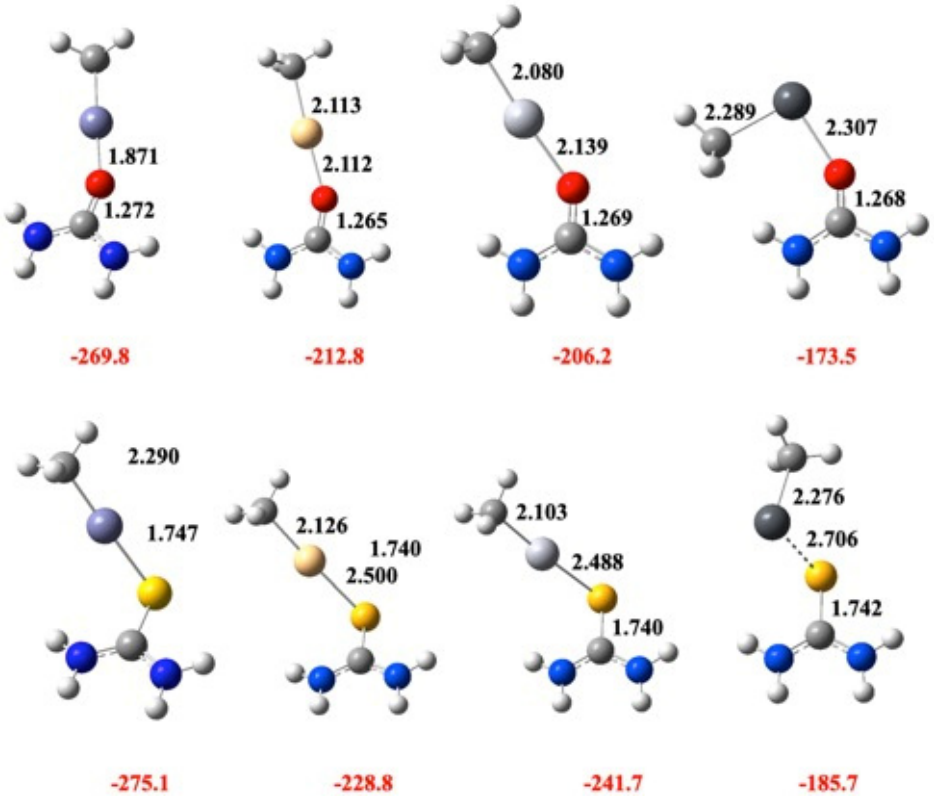

Figure 4. Optimized geometries of the complexes between urea (first row) and thiourea (second row) with CH_3M^+ (M = Zn, Cd, Hg, Pb) monocations. Bond lengths are in Å. The calculated binding energies for the different complexes (in $kJ \cdot mol^{-1}$) are given in red.

There are however some subtle differences with respect to the dications, mainly in what concerns the trends observed for the CH_3M^+ binding energies. Indeed, although like for the dications (Table 3) the largest charge transfer energy for the monocations (see Table 4) is also found for mercury (see Table 4), the CH_3Hg^+ binding energies are always smaller than those of CH_3Zn^+, and even slightly smaller than the CH_3Cd^+ for the particular case of urea (see Figure 4).

Table 4. Calculated NBO-NEDA charge transfer energies ($kJ \cdot mol^{-1}$) between urea and thiourea with CH_3M^+ (M = Zn, Cd, Hg, Pb) metal monocations.

	Urea	Thiourea
CH_3Zn^+	-233.5	-378.6
CH_3Cd^+	-179.1	-320.8
CH_3Hg^+	-259.8	-414.7
CH_3Pb^+	-215.0	-359.7

Our interpretation is that the relativistic contraction of the Hg orbitals responsible for the enhanced intrinsic Lewis acidity of Hg^{2+} cations is very much attenuated in these complexes by the methyl group attached to the metal. A detailed analysis of this question would require further investigation, as preliminary experimental results obtained by our group indicate significant differences between the reactivity of the CH_3Hg^+ ions towards urea or thiourea. As illustrated in Figure S3, the $[CH_3Hg(urea)]^+$ ion (*m/z* 277 with ^{202}Hg) could not be generated under electrospray conditions (Figure S3a) , whereas replacing urea by thiourea results, under similar experimental conditions, in a very simple mass spectrum, almost exclusively composed of the $[CH_3Hg(thiourea)]^+$ complex (*m/z* 293). This is consistent with the high sequestering power observed in solution for the S donor ligand as compared to the oxygen of nitrogen-containing ligand.[57]

The role of the R alkyl chain in the reactivity of RHg^+

We highlighted in the Introduction the environmental importance of the reactivity of methyl mercury. In the results commented so far, we have paid attention to the nature of the metal. Now, we wonder about the importance of the alkyl chains accompanying such metals. In a previous work, we studied the processes associated with the complexation between uracil and two alkyl mercury cations of different lengths, methyl mercury and n-butyl mercury, performed in the gas phase through electrospray ionization coupled to tandem mass spectrometry.[58] Very importantly, the length of the chain was shown to be crucial for the final products observed in the laboratory, being predominantly methyl uracil cation in the first case (methylation occurring onto the carbonyl group(s) of uracil according to InfraRed Multiple Photon Dissociation experiments), and protonated

uracil in the second case. Our hypothesis, supported by theoretical studies, is that the different behavior is due to the flexibility of the butyl group, which allows a different pathway for a proton transfer towards uracil and the corresponding elimination of mercury and alkyl residues. These results opened the question of the performance of an intermediate-size alkyl group such as the ethyl group when associated with uracil, and this is the topic we are going to analyze in this section.

We have explored a large set of isomers, including different conformational orientations, for the fragmentation process of the complexes formed between uracil and ethyl mercury cation. The most relevant $[EtHg(U)]^+$ and $[UEt]^+$ structures (U = uracil, Et = ethyl chain) were obtained at the B3LYP level using a 6-31++G(d,p) basis set for all atoms except Hg, for which the DEF2-TVZPPD was chosen. The latter basis set includes a small core pseudopotential to account for relativistic effects.

As a first step, we identified the most stable isomers of the different compounds involved in the reactions, shown in Figures 5 and 6. A scheme accounting for the labeling code used for the structures is included in the pictures, where U stands for uracil, numbering 1-6 is related to the position in the ring, labels [a, b, c, d] are related to the orientation of the substituent atom (H) or alkyl chain leading to different conformers, and characters E and dE, if present, mean enolic or dienolic forms.

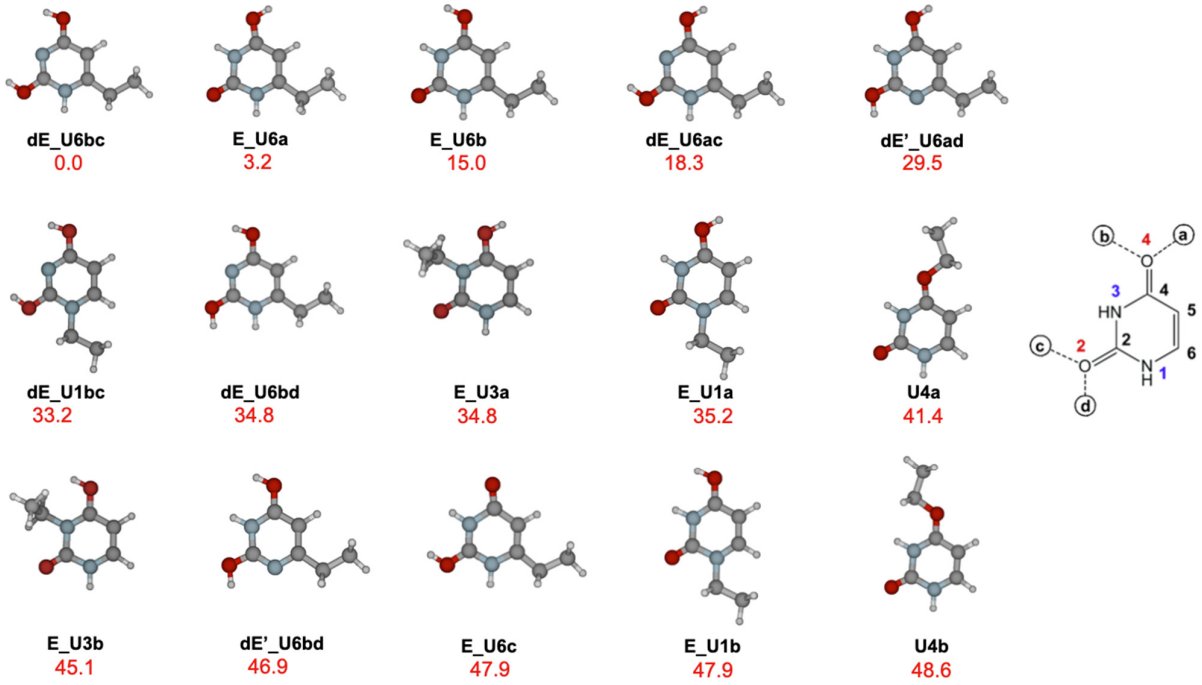

Figure 5. Most stable ethyl uracil cations. Relative enthalpies ($kJ \cdot mol^{-1}$) are shown in red color. See also Table S1.

The isomers for the different uracil protonated structures were already available from our previous investigations,[58] whereas the ethyl uracil and ethylmercury uracil cations were obtained for the present work. The uracil molecule presents several O, N and C binding sites, from which the ones leading to the most stable structures are carbon C6 in the case of the ethyl chains (Figure 5) and the oxygen atoms O4 and O2 in the case of the ethyl-mercury chains (Figure 6). The relative stabilities of the isomers comprised between 0 and 50 kJ/mol are also shown, whereas the whole lists of isomers with their corresponding energies can be consulted in Tables S1-S2.

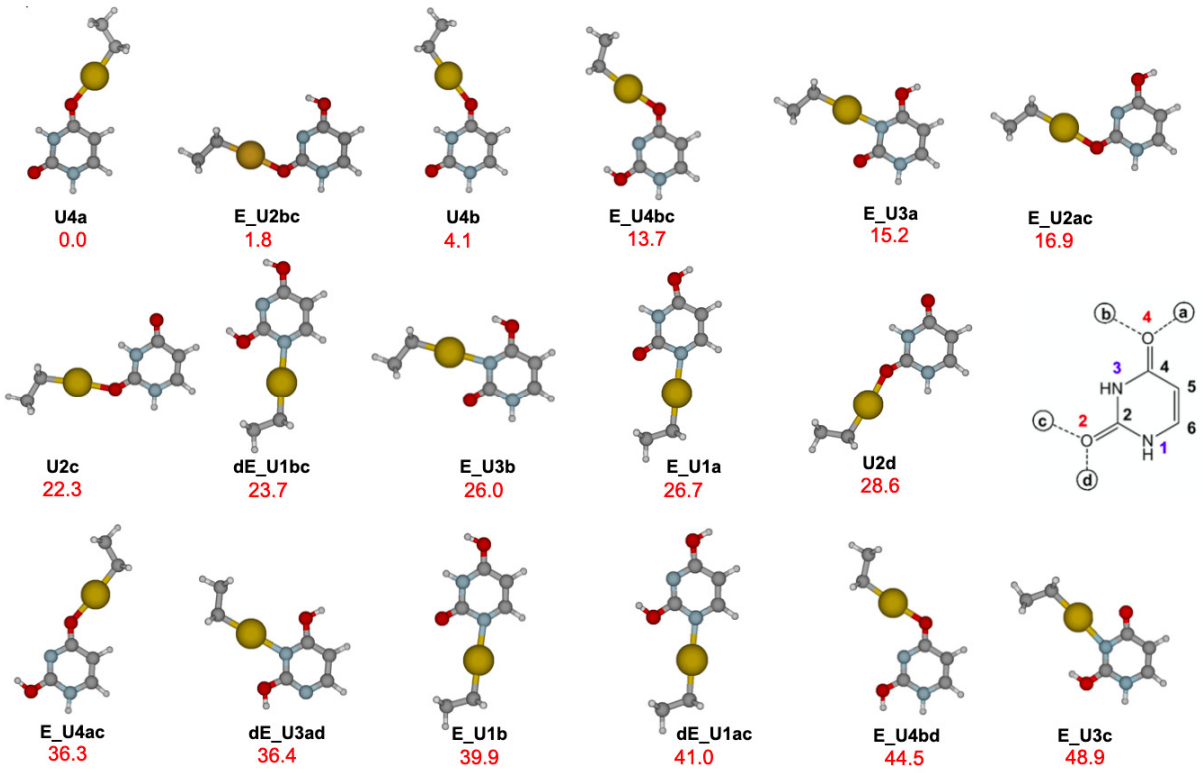

Figure 6. Most stable $[EtHg(U)]^+$ cations. Relative enthalpies ($kJ \cdot mol^{-1}$) are shown in red color. See also Table S2.

As a strategy to find the products resulting from the attachment of the ethyl mercury cation to uracil, we decided to explore three different mechanisms starting from $[EtHg(U)]^+$, which should be the first complex formed between the interacting species. The three mechanisms are the following: (i) a beta-hydride elimination from the alkyl mercury chain, which would lead to $[UHgH]^+$ and ethene; (ii) an alkyl transfer to uracil,

leading to [UEt]+ and mercury ^{0}Hg, and (iii) a proton transfer to uracil, resulting in $[UH]^{+}$, mercury and ethene. The key transition states found for the three paths are connected to a $[EtHg(U)]^{+}$ isomer, **E_U4bc** (see Figure 6), which is not the most stable ethylmercury uracil isomer but can be reached from an internal proton transfer. This previous isomerization reaction is shown in Figure 7.

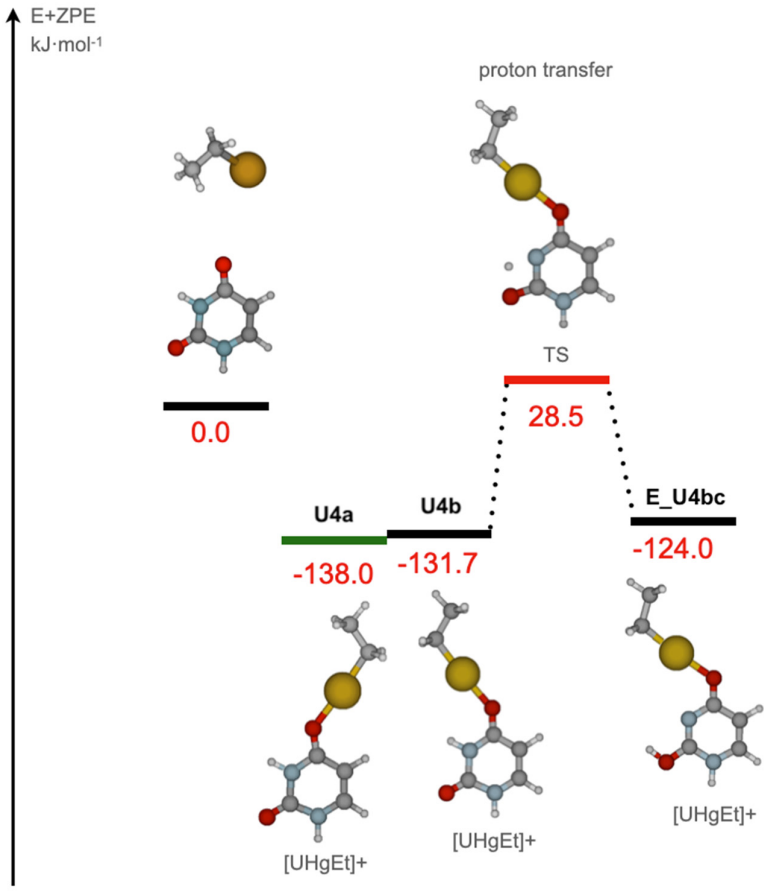

Figure 7. Isomerization from isomer **U4b** to reach isomer **E_U4bc** through an internal proton transfer. Relative energies plus zero-point energy ($kJ \cdot mol^{-1}$) are shown in red color.

The three abovementioned paths (i), (ii) and (iii) starting from ethyl mercury uracil isomer **E_U4bc** are described in Figures 8 and 9, respectively.

As can be immediately noticed, the beta-hydride elimination (i) in Figure 8 requires overcoming a transition state located 217 kJ·mol^{-1} above the reagents and, moreover, the products $[UHgH]^+$ and ethene are slightly below the entrance channel (-25 kJ·mol^{-1}). These ionic products were not observed experimentally. However, an ulterior proton transfer from $[UHgH]^+$ could eventually lead to protonated uracil and the elimination of mercury (Figure S4), but again with a very high barrier as a consequence of the distorted geometry of the O-Hg-H angle in the transition state structure. Therefore, our conclusion is that path (i) should not be, in principle, the one preferred to reach the observed products.

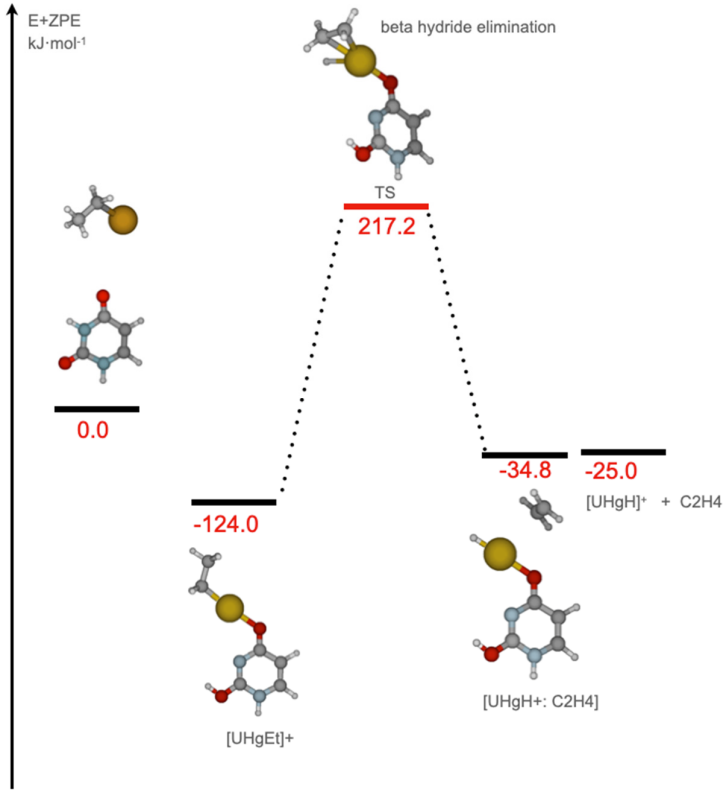

Figure 8. Beta-hydride elimination from $[EtHg(U)]^+$ to $[UHgH]^+$ plus ethene. Relative energies plus zero-point energy (kJ·mol^{-1}) are shown in red color. See also Figure S4.

Instead, mechanisms (ii) and (iii) are much more feasible according to the computed energy profiles. Figure 9 describing mechanism (ii) shows an exothermic alkyl transfer from the alkyl mercury chain towards oxygen from uracil, resulting in a very

stable $[UEt]^+$ product (-175 kJ/mol with respect to the entrance channel). The same figure illustrates mechanism (iii), with an even lower barrier and leading to protonated uracil (-95 kJ/mol below the reagents). From these profiles, protonated uracil would be a kinetic product, whereas ethyl uracil would be the thermodynamic product.

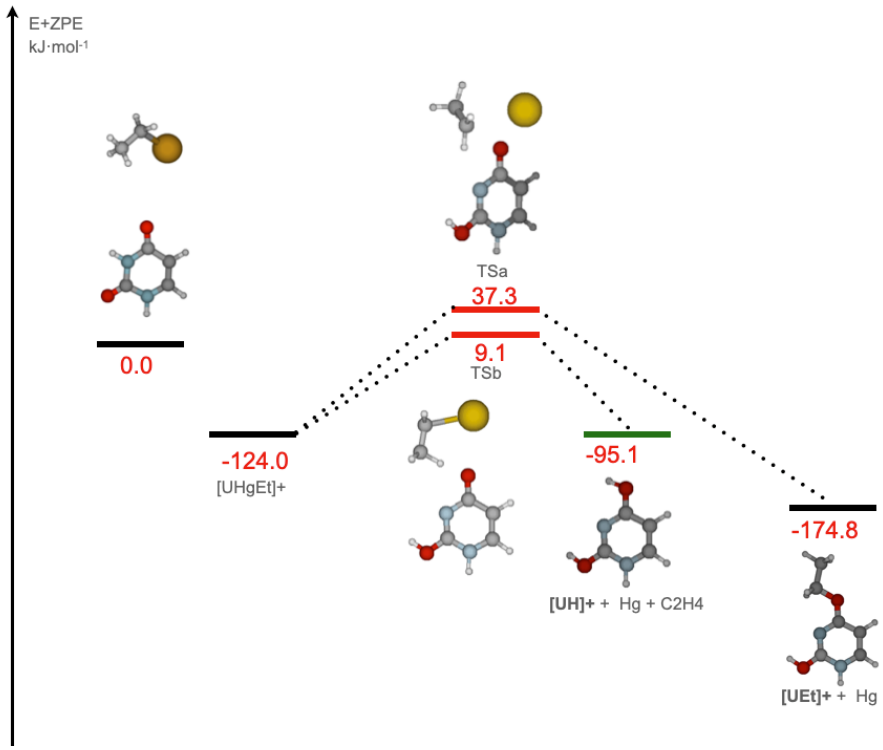

Figure 9. Potential energy profiles associated with mechanism (ii), the ethyl chain transfer (**TSa**) to uracil, leading to $[UEt]^+$ and mercury ^0Hg, and mechanism (iii), a proton transfer to uracil (**TSb**), resulting in $[UH]^+$, mercury and ethene. Relative energies plus zero-point energy ($kJ \cdot mol^{-1}$) are indicated in red.

Globally, these two mechanisms are very similar in terms of energy path (see Figure 9), and the two fragment ions are observed experimentally (Figure 10b) with comparable intensities. When going back to the CH_3Hg^+/uracil system, the mechanism (iii) should not be accessible as it would imply a very constrained transition state and a high activation barrier. Logically, protonation of uracil is not observed in the MS/MS spectrum (Figure 10a).

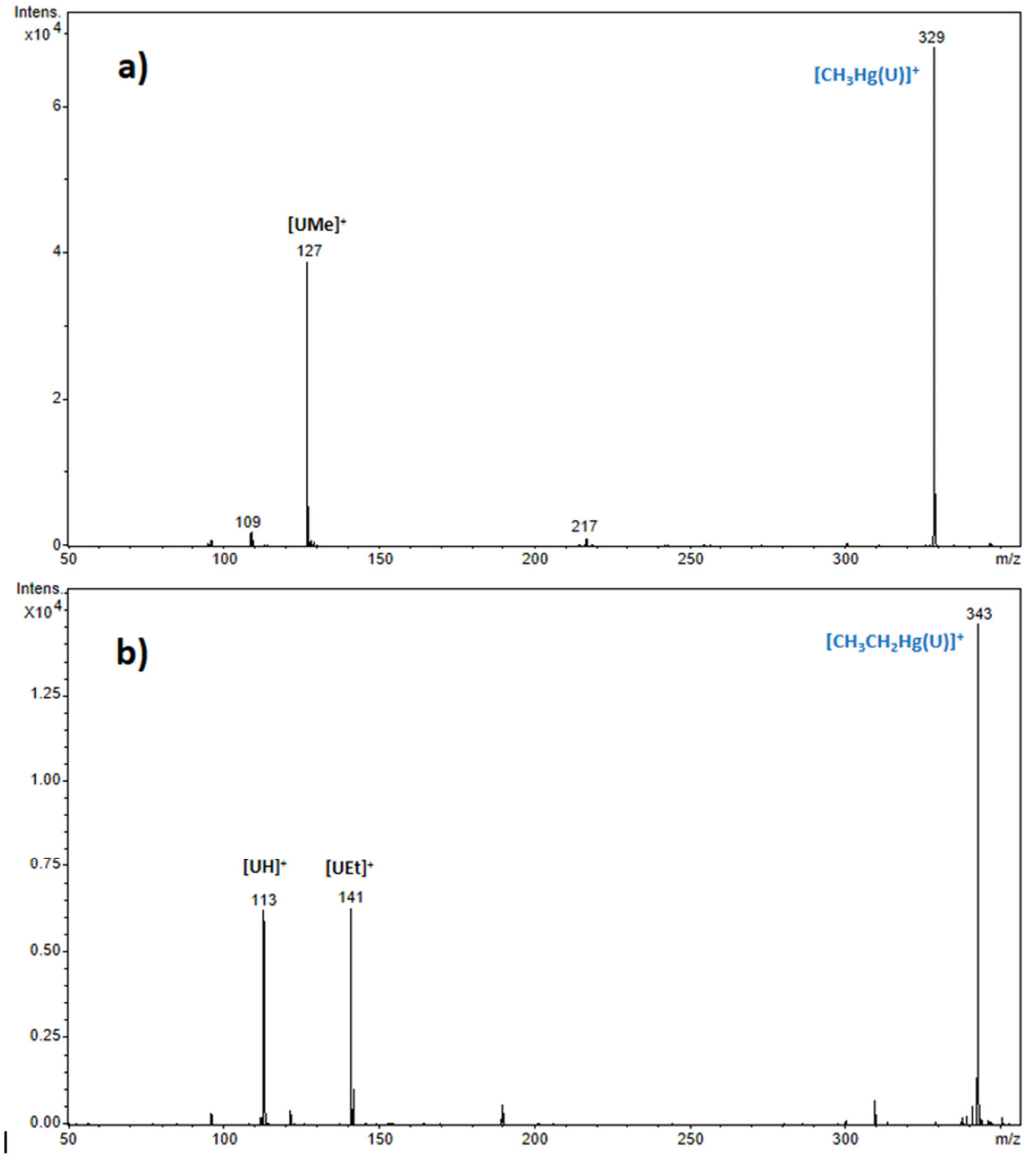

Figure 10. MS/MS spectra of a) the $[CH_3Hg(U)]^+$ (*m/z* 329) and b) $[CH_3CH_2Hg(U)]^+$ (*m/z* 343) complexes recorded on Bruker Amazon HCT 3D ion trap (equimolar solution of RHgCl and uracil (10^{-4}M) in a water/methanol mixture (50/50 v/v)), with a fragmentation time of 40 ms and a fragmentation amplitude of 0.7V.

It is worth mentioning that the transition state **TSb** in Figure 9 was not considered in our previous theoretical study regarding the reactivity between the n-butylmercury cation and uracil.[58] Once this structure was located for the $EtHg^+$/uracil system, we searched for a similar transition state for the butyl case. This new transition state is found

19.7 kJ·mol^{-1} above the entrance channel and leads to protonated uracil plus mercury and 1-butene, which are the result of an exothermic process (-95.9 kJ·mol^{-1}). This mechanism is therefore much more favorable than the one postulated in our previous publication, and more in line with the dominant protonation of uracil as compared to butyl transfer.[58] The dominant protonation path is also consistent with the transition state associated with the butyl chain transfer located 83.2 kJ mol^{-1} above the reactants, and therefore well above the one found for proton transfer. Finally, it is worth noting that the observation in the gas phase of the dienolic form of protonated uracil shown in Figure 9, has been evidenced by IRMPD experiments.[59]

In summary, although taking into account that the experimental conditions leading to products are not directly comparable with the equilibrium geometries described in the energy reaction profiles, two transition states were found that account for the production of ethyl uracil cation and protonated uracil and would explain the different ratios observed. Taking into account the previously reported results and the new ones, the ethyl mercury cation study contributed to provide new answers regarding the importance of the length of the alkyl chain attached to the metal. For methyl mercury, only the alkyl transfer is allowed. For ethyl mercury, both paths are competitive experimentally. For butyl mercury, protonation is clearly dominant, in agreement with past and present results. All these considerations are summarized in Figure 11.

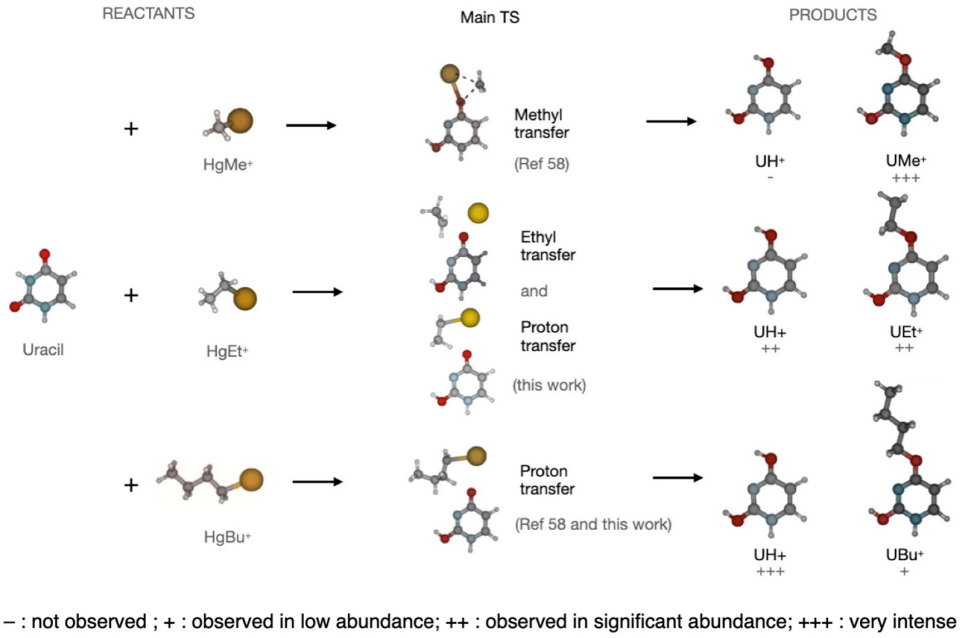

Figure 11. Summary of the main results regarding the reactivity of [RHg]$^+$ and uracil. To facilitate the comparison between the products, we have used the same isomers in the scheme.

To conclude this section, it is important to mention that the nucleobase alkylation process would also deserve a computational reinvestigation, as the mechanism described here could compete with an S_N2-like mechanism, like the one described for the methylation of ammonia by MCH_3^+ ions (M=Zn, Cd, Hg) by H. Schwarz and co-workers.[60] Applied to the present systems, this mechanism would start from a complex between uracil and the $[RHg]^+$ ion, where the nucleobase binds the cation through the alkyl group instead of Hg. However, the description of the associated PES still represents a challenge for modern computational methods as far as alkylmercury ions $[RHg]^+$ are concerned.

Concluding remarks

The ionic forms of heavy metals cadmium, mercury and lead are able to strongly bind nitrogen and carbonyl oxygen basic sites of biomolecular systems, although the relative strength of the interactions and preferred binding sites are quite different. The study of the structures, energies and different energy terms contributing to the total interaction between M^{2+} ions and urea and thiourea as model systems, have shown stronger interactions with thiourea. According to EDA, this is due to a larger contribution of the polarization energy term with respect to the electrostatic one, to the point that in thiourea systems a covalent bond is formed, resulting in bond orders higher than 1. The preference for thiourea is particularly enhanced in the case of mercury, in line with the EDA and NEDA results which indicate for this ion the largest charge transfer of all the systems studied. Moving from M^{2+} ions to RM^+ ions, our preliminary calculations show that the interactions with urea and thiourea are also very large, but lower than in the previous case. In this sense, it is still an open question that deserves further investigation why $[CH_3Hg(urea)]^+$ is not generated under electrospray conditions, whereas the $[CH_3Hg(thiourea)]^+$ complex is readily observed. Finally, we have studied the influence of the length of the alkyl chain on the reactivity of $[RHg]^+$ ions towards uracil. The proposed mechanisms are able to explain the product ions observed experimentally, where the increasing number of carbons of the alkyl chain makes the proton transfer process more likely than the alkyl chain transfer. It is still a challenge to find if an S_N2-like mechanism could play a role in the alkyl mercury reactivity towards nucleobases.

Acknowledgements

This work was carried out with financial support from the projects PID2021-125207NB-C31, PID2021-125207NB-C32 and PID2019-110091GB-I00 of the Ministerio de Ciencia, Innovación y Universidades of Spain (MICI NN), and the PRIES-CM project Y2020/EMT-6290 from the Comunidad Autónoma de Madrid. J.Y Salpin would like to thank the ANR CHARMMMAT (ANR11-LABX-0039) for the financial support allowing the acquisition of the 3D ion trap instrument. We are grateful to Prof. Marcos Mandado (Universidade de Vigo, Spain) for his kind help and fruitful discussions. Á. Pérez-Barcia thanks Universidade de Vigo for the predoctoral fellowship P.P. 00VI 131H 6410211. M. M. Montero-Campillo would like to thank the Ministerio de Universidades and the Universidad Autónoma de Madrid for her ARPU (Ayudas para la Recualificación del Profesorado Universitario) fellowship at the Universidade de Vigo (Spain), which is financially supported by the Plan de Recuperación, Transformación y Resiliencia 2020. Finally, the authors thank the Centro de Computación Científica of the UAM (CCC-UAM) for the generous allocation of computer time and continued technical support.

Bibliography

1. H. J. Lee, M. K. Park and Y. T. Seo, *Toxicol. Environ. Health. Sci.*, 2018, **10**, 1-10.
2. M. Jaishankar, T. Tseten, N. Anbalagan, B. B. Mathew and K. N. Beeregowda, *Interdiscipl. Toxicol.* , 2014, **7**, 60-72.
3. M. Fleischer, A. F. Sarofim, D. W. Fassett, P. Hammond, H. T. Shacklette, I. C. Nisbet and S. Epstein, *Environ. Health Perspect.*, 1974, **7**, 253-323.
4. V. Hiatt and J. E. Huff, *Int. J. Environ. Stud.*, 1975, **7**, 277-285.
5. J. Emsley, *The Elements* Clarendon Press, Oxford, 1998.
6. P. B. Tchounwou, C. G. Yedjou, A. K. Patlolla and D. J. Sutton, in *Molecular, Clinical and Environmental Toxicology*, ed. A. Luch, Springer, Basel2012, vol. 101.
7. D. Ohms, M. Kohlhase, G. Benczur-Urmossy and G. Schadlich, *J. Power Sources*, 2002, **105**, 127-133.
8. L. Jarup, *Nephrol. Dial. Transplant.*, 2002, **17**, 35-39.
9. E. Mitchell, S. Frisbie and B. Sarkar, *Metallomics*, 2011, **3**, 874-908.
10. S. Satarug and M. R. Moore, *Environ. Health Perspect.*, 2004, **112**, 1099-1103.
11. V. Verougstraete, D. Lison and P. Hotz, *Mutat. Res. Rev. Mutat. Res.*, 2002, **511**, 15-43.
12. M. Waisberg, P. Joseph, B. Hale and D. Beyersmann, *Toxicology*, 2003, **192**, 95-117.
13. T. Nawrot, M. Plusquin, J. Hogervorst, H. A. Roels, H. Celis, L. Thijs, J. Vangronsveld, E. Van Hecke and J. A. Staessen, *Lancet Oncol.*, 2006, **7**, 119-126.

14. I. Onyido, A. R. Norris and E. Buncel, *Chem. Rev.*, 2004, **104**, 5911–5929.
15. M. Israr, S. Sahi, R. Datta and D. Sarkar, *Chemosphere*, 2006, **65**, 591-598.
16. A. Maggio and R. J. Joly, *Plant Physiol.*, 1995, **109**, 331–335.
17. T. W. Clarkson, L. Magos and G. J. Myers, *New Eng. J. Med.*, 2003, **349**, 1731–1737.
18. M. R. Karagas, A. L. Choi, E. Oken, M. Horvat, R. Schoeny, E. Kamai, W. Cowell, P. Grandjean and S. Korrick, *Environ. Health Perspect.*, 2012, **120**, 799-806.
19. Y. S. Hong, Y. M. Kim and K. E. Lee, *J. Prev. Med. Public Health*, 2012, **45**, 353–363.
20. J. L. Franco, T. Posser, P. R. Dunkley, P. W. Dickson, J. J. Mattos, R. Martins, A. C. D. Bainy, M. R. Marques, A. L. Dafre and M. Farina, *Free Radic. Biol. Med.*, 2009, **47**, 449-457.
21. P. A. Nogara, C. S. Oliveira, G. L. Schmitz, P. C. Piquini, M. Farina, M. Aschner and J. B. T. Rocha, *Biochim. Biophys. Acta Gen. Subj.*, 2019, **1863**.
22. H. A. Waldron, *Med. Hist.* , 1973, **17**, 391-199.
23. M. A. Riva, A. Lafranconi, M. I. D'orso and G. Cesana, *Saf. Health Work*, 2012, **3**.
24. M. Hanna-Attisha, J. LaChance, R. C. Sadler and C. S. A., *Am. J. Public Health*, 2016, **106**, 283-290.
25. D. Rosner, G. Markowitz and B. J. Lanphear, *Public Health Rep.*, 2005, **120**, 296-300.
26. J. N. Harvey, *Annu. Rep. Prog. Chem., Sect. C,*, 2006, **102**, 203-226.
27. R. Ferreiros-Martinez, D. Esteban-Gomez, C. Platas-Iglesias, A. de Blas and T. Rodriguez-Blas, *Dalton Trans.*, 2008, 5754-5765.
28. K. Liu, W. Shi and P. Cheng, *Dalton Trans.*, 2011, **40**, 8475-8490.
29. N. S. Sisombath, F. Jalilehvand, A. C. Schell and Q. Wu, *Inorg. Chem.*, 2014, **53**, 12459-12468.
30. Y. Z. Niu, J. Y. Yang, R. J. Qu, Y. H. Gao, N. Du, H. Chen, C. M. Sun and W. X. Wang, *Ind. Eng. Chem. Res.* , 2016, **55**, 3679-3688.
31. B. C. Shepler and K. A. Peterson, *J. Phys. Chem. A*, 2003, **107**, 1783-1787.
32. M. Filatov and D. Cremer, *Chemphyschem*, 2004, **5**, 1547-1557.
33. J. A. Tossell, *J. Phys. Chem. A*, 2006, **110**, 2571-2578.
34. T. Bollermann, T. Cadenbach, C. Gemel, M. von Hopffgarten, G. Frenking and R. A. Fischer, *Chem.-Eur. J.*, 2010, **16**, 13372-13384.
35. M. Enescu and A. Manceau, *Theor. Chem. Acc.*, 2014, **133**, 1457.
36. S. Roy, K. C. Mondal and H. W. Roesky, *Acc. Chem. Res.*, 2016, **49**, 357-369.
37. R. Saha, S. Pan, P. K. Chattaraj and G. Merino, *Dalton Trans.*, 2019, **49**, 1056-1064.
38. S. Pan, L. L. Zhao and G. Frenking, *Theor. Chem. Acc.*, 2021, **140**, 69.
39. M. S. Liao, Q. E. Zhang and W. H. E. Schwarz, *Inorg. Chem.*, 1995, **34**, 5597-5605.
40. A. F. Khalizov, B. Viswanathan, P. Larregaray and P. A. Ariya, *J. Phys. Chem. A*, 2003, **107**, 6360-6365.
41. E. Kraka and D. Cremer, *Int. J. Mol. Sci.*, 2008, **9**, 926-942.
42. D. Cremer, E. Kraka and M. Filatov, *Chemphyschem*, 2008, **9**, 2510-2521.
43. E. Pahl, D. Figgen, A. Borschevsky, K. A. Peterson and P. Schwerdtfeger, *Theor. Chem. Acc.*, 2011, **129**, 651-656.
44. S. Evangelisti, G. L. Bendazzoli and L. Gagliardi, *Chem. Phys.*, 1994, **185**, 47-56.

45. M. W. Schmidt, J. Ivanic and K. Ruedenberg, *J. Phys. Chem. A*, 2010, **114**, 8687-8696.
46. M. El Khatib, G. L. Bendazzoli, S. Evangelisti, W. Helal, T. Leininger, L. Tenti and C. Angeli, *J. Phys. Chem. A*, 2014, **118**, 6664-6673.
47. M. M. Montero-Campillo, O. Mó, M. Yáñez, I. Alkorta and J. Elguero, *Adv. Inorg. Chem.*, 2019, **73**, 73-121.
48. J. A. Tossell, *J. Phys. Chem. A*, 1998, **102**, 3587-3591.
49. A. Madabeni, M. Dalla Tiezza, F. B. Omage, P. A. Nogara, M. Bortoli, J. B. T. Rocha and L. Orian, *J. Comput. Chem.*, 2020, **41**, 2045-2054.
50. E. D. Glendening, *J. Am. Chem. Soc.*, 1996, **118**, 2473-2482.
51. E. D. Glendening, *J. Phys. Chem. A*, 2005, **109**, 11936-11940.
52. E. D. Glendening, J. K. Badenhoop, A. E. Reed, Carpenter, J. E. Bohmann, J. A. Morales and F. C. M.; Weinhold, Theoretical Chemistry Institute, University of Wisconsin. *NBO 5.G*, Madison, WI, 2004.
53. A. Zuttel, S. Rentsch, P. Fischer, P. Wenger, P. Sudan, P. Mauron and C. Emmenegger, *J. Alloys Compds.*, 2003, **356**, 515-520.
54. M. Mandado and J. M. Hermida-Ramón, *J. Chem. Theory Comp.*, 2011, **7**, 633-641.
55. N. Ramos-Berdullas, I. Perez-Juste, C. Van Alsenoy and M. Mandado, *Phys. Chem. Chem. Phys.*, 2015, **17**, 575-587.
56. R. D. Shannon, *Acta Crystallogr. A*, 1976, **32**, 751-767.
57. G. Falcone, C. Foti, A. Gianguzza, O. Giuffre, A. Napoli, A. Pettignano and D. Piazzese, *Anal. Bioanal. Chem.*, 2013, **405**, 881-893.
58. J. Y. Salpin, V. Haldys, L. Latrous, J. C. Guillemin, J. Tortajada, E. Leon, O. Mó, M. Yáñez and M. M. Montero-Campillo, *Int. J. Mass Spectrom.*, 2019, **436**, 153-165.
59. J. Y. Salpin, S. Guillaumont, J. Tortajada, L. MacAleese, J. Lemaire and P. Maitre, *Chemphyschem*, 2007, **8**, 2235-2244.
60. R. Kretschmer, M. Schlangen, M. Kaupp and H. Schwarz, *Organometallics*, 2012, **31**, 3816-3824.

Graphical Abstract

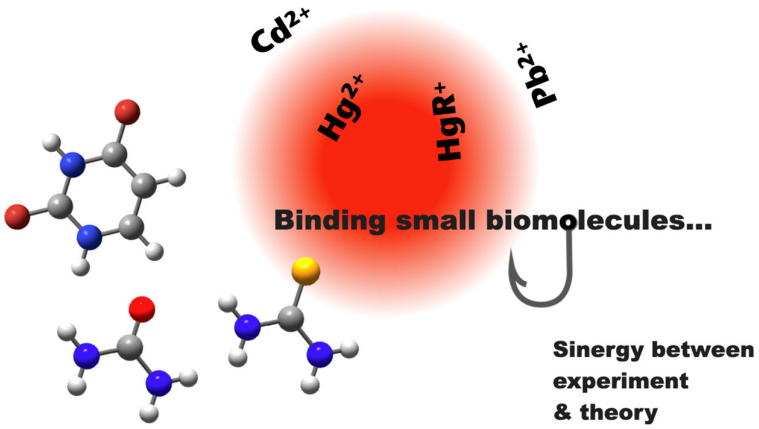
Cd^{2+}
Hg^{2+}
HgR^{+}
Pb^{2+}
Binding small biomolecules...
Sinergy between
experiment
& theory

Open questions on toxic heavy metals Cd, Hg and Pb binding small components of DNA and nucleobases. Are there any predictable trends?

Álvaro Pérez-Barcia, M. Merced Montero-Campillo, Al Mokhtar Lamsabhi, Jean-Yves Salpin, Manuel Yáñez

Departamento de Química Física, Universidad de Vigo, Lagoas-Marcosende s/n,36310 Vigo, Spain; Departamento de Química, Módulo 13, Facultad de Ciencias, and Institute of Advanced Chemical Sciences (IAdChem), Universidad Autónoma de Madrid, Campus de Excelencia UAM-CSIC, Cantoblanco, 28049 Madrid, Spain; Université Paris-Saclay, Univ Evry, CNRS, LAMBE, 91025, Evry-Courcouronnes, France; LAMBE, CY Cergy Paris Université, CNRS, 95000 Cergy, France

Supporting Information
CONTENTS

Bibliographic compilation of experimental and theoretical work on Cd, Hg and Pb.

Cd

Cadmium is categorized as a non-essential element since it is not naturally involved in any physiological process. However, although its ionic radius is larger (~0.18 Å), it is chemically similar to zinc and often replaces it in binding sites of enzymes and proteins. The binding of Cd to proteins is therefore one of the reasons for its toxicity**,** thereby inhibiting important physiological functions.[1, 2] This is the case for example of zinc finger proteins which are involved in DNA repair. Zinc finger proteins are characterized by Zn^{2+} ions interacting preferentially with cysteine (Cys) and histidine (His) residues, and the particularly high affinity of toxic metals such as Cd for thiol groups, make cysteine-containing zinc finger proteins particularly susceptible to Zn^{2+} replacement. Zn replacement by Cd inactivates these proteins, which can no longer bind to DNA.[3] Exposure to cadmium also promotes the synthesis of metallothioneins (MT)[4], which are a class of cysteine-rich proteins playing a role in the protection against metal toxicity and oxidative stress, and which have the capability to bind cadmium through their Cys residues.[5, 6]

The importance of the substitution of Zn by Cd in proteins has therefore motivated numerous experimental and/or theoretical studies about the interactions of cadmium with amino acids, proteins and relevant model compounds. Performing these studies in the gas phase allows the description of these interactions at the molecular level and can give access to the intrinsic properties of such interactions in the absence of solvation and counter-ion effects. Those that have been carried out during the three last decades, are briefly summarized in this section.

Given the key role played by the cysteine residue, a peculiar attention was given to the interactions between cadmium and this amino acid. In 2005, Belcastro and co-workers[7] published a detailed computational study about the doubly-charged M^{2+}-cysteine complex (M=Cu, Zn, Cd , Hg). To this end, calculations were carried out in the framework of density functional theory (DFT), and different binding schemes were considered, including both neutral and zwitterionic forms, the latter being often strongly stabilized when complexed with metal ions. Their study showed that Zn^{2+} and Cd^{2+} ions share the same preferred binding scheme, characterized by a tridentate interaction involving the carbonyl oxygen, nitrogen and sulfur atoms of neutral cysteine. It is similar to that found both experimentally and theoretically for Li^+ and Na^+,[8, 9] whereas different

types of complexes coexist for heavier alkali metals.[9] On the other hand, this binding scheme turned to be different than that computed for Cu^{2+} and Hg^{2+}, which implied a zwitterionic form of cysteine. Note that a more recent DFT study using a larger basis set than LANL2DZ, also found for Cd^{2+} a global minimum involving zwitterionic cysteine, characterized by a bidentate interaction with the carbonyl oxygen and the deprotonated thiol group.[10] This discrepancy was attributed to the larger basis set superposition error associated with the LANL2DZ.

When studying the gas-phase interactions between transition metals and aminoacids by mass spectrometry, both the type and the stoichiometry of the complexes observed experimentally may strongly depend on the type of salts used to prepare the solutions, but also on the ionization source used. But generally, when using electrospray ionization (ESI), the interactions taking place with dications are associated with deprotonation of the amino acid. This had been shown twenty years ago for example for Zn^{2+} ions by the group of Ohanessian with glycine, asparagine or aspartic acid.[11-13]. Later, Burford and co-workers[14] studied the complexes generated by electrospray between a series of toxic metal ions (and notably cadmium and mercury), with the whole series of aminoacids (aa). The observed spectra were found independent of the reaction mixture stoichiometry (10:1 – 1:10). Starting from nitrate salts, they observed deprotonated amino acids complexes with Hg^{2+} and Cd^{2+}. Remarkably, with cadmium, complexes of general formula $[Cd(aa)+X]^+$ ($X=NO_3^-$), that is formally involving an intact amino acid, were observed with all the amino acids but histidine and asparagine. Similar complexes involving neutral aminoacids can also be generated starting from chloride salts ($X=Cl^-$), as shown by the studies carried out by the group of P. B Armentrout (*vide infra*).[15-25] Burford and co-workers also examined the interactions taking place with the tripeptide glutathione (GSH: γ-Glu–Cys–Gly).[26] With Cd, a very intense $[Cd(GSH)-H]^+$ complex is observed. Interestingly, the MS/MS spectrum of this complex shows only product ions retaining the thiolate group, indicative of the strong affinity of cadmium for thiolates. Ternary equimolar mixtures of $Cd(NO_3)_2$ and two biologically relevant thiol amino acids R_1SH and R_2SH have been also studied by ESI-MS.[27] Again, deprotonation occurred and complexes of the type $[Cd(R_1SH)(R_2SH),-H]^+$ were generated by electrospray. Interestingly, the theoretical 1:2:1 intensity ratio expected for homodimers and heterodimers was not observed, suggesting some degree of discrimination between the different thiols. Authors also noticed that the intensities of the complexes were much less

intense than those obtained with Hg^{2+} under similar conditions[28], pointing to a higher affinity of mercury for thiolates.

In these two previous experimental studies dealing with Cd^{2+} interactions, authors assumed an interaction with deprotonated sulfur to interpret their MS/MS spectra. Furthermore, Rubino and co-workers suggested for their dimers a linear S-Cd-S geometry. The first assumption sounds reasonable according to several theoretical reports on model compounds. For instance, a study published in 2000 by Rulíšek and Havlas, in which side chains of amino acids were replaced by functional groups, showed that the interaction energies of negatively charged residues (deprotonated amino acid side chains) were by one order of magnitude greater than those of the neutral species.[29] This theoretical study gives also support to the second assumption, as linear coordination geometry turned to be especially favorable for soft metal ions such as Cd(II) and Hg(II). A theoretical study about the interactions between group 12 metal $M_n(H_2O)^{2+}$ (n=0-2) ions and deprotonated cysteine has been carried out by Mori and co-workers.[10] While the lack of water molecule (n=0) resulted in the loss of CO_2 during the optimization step, the most stable forms optimized when the complexes are microsolvated by one or two molecules of water, systematically implied deprotonation of the thiol group. For one water ligand, that this for the $[M(H_2O)(Cys\text{-}H)]^+$ complex, a similar tridentate $[O,N,S^-]$ coordination scheme involving the carbonyl oxygen, the nitrogen and deprotonated sulfur was found for Zn^{2+}, Cd^{2+} and Hg^{2+}. The amount of charge transfer to the metal is much more pronounced for Hg than for Cd or Zn, (+0.90e, +1.37e, +1.41e, respectively). Adding a second water ligand or using a polarized continuum model resulted in a preferred bidentate conformation for Cd and Hg (N,S^-), whereas Zn remains tricoordinated. Mori and co-workers also estimated the binding energy of the bare dications with neutral cysteine and found the following order Zn(II)> Hg(II)>Cd(II), in agreement with a previous study.[7] The estimated values turned to be significantly larger with the B3LYP functional as compared to CCSD(T) calculations. This trend was later confirmed by Ahlstrand et al.[30], who compared the binding energy computed by four different functionals (B3LYP, B98, TPSSh, M06) to CCSD(T) estimates, for complexes of Zn^{2+} or Cd^{2+} with amino acid mimics (acetate, methanethiolate, and imidazole) or water.

Whereas DFT functionals overestimate the magnitude of the interaction energy, on the other hand they correctly predict the structure of the complexes generated in the gas phase by the interaction of Zn^{2+} or Cd^{2+} with a single amino acid (aa), as evidenced

by numerous combined theoretical/IRMPD (InfraRed Multiple Photon Dissociation) studies. IRMPD spectroscopy of mass-selected ion is now established as a powerful approach for the structural characterization of gaseous metal ions/biomolecules complexes.[31-34] P. B. Armentrout and co-workers have carried out an extensive study about the interactions taking place in the gas phase between Zn^{2+}, Cd^{2+} and a series of aminoacids.[15-25, 35-37] Regardless the type of complexes generated by electrospray, namely $[Cd(aa)-H]^+$ or $[CdCl(aa)]^+$, these studies show that a systematic agreement is observed between the DFT-computed ground state and the experimental IRMPD spectra, and that Cd interacts through a tridentate binding scheme with a charge-solvated form of the amino acid, involving the backbone nitrogen, the oxygen of the carbonyl of the carboxylic group and a heteroatom of the side chain. In several studies, the same complexes could be observed for both Zn and Cd. This is the case of the $[Zn(aa)-H]^+$ and $[Cd(aa)-H]^+$ ions (aa=Cys, His),[15, 16] or $(MCl(Met)]^+$,[25] and the two metals are found to share the same binding scheme, with shorter interacting distances for Zn due to smaller ionic radius and stronger electrostatic interactions. This is illustrated for instance by the $[Zn(cys)-H]^+$ and $[Cd(cys)-H]^+$ ions, which could be generated from acetonitrile adducts produced by electrospray and irradiated by a continuous wave CO_2 laser. These two complexes exhibit similar IRMPD action spectra which are in very good agreement with tridentate conformers involving thiol group deprotonation, like those found previously.[10] The same tridentate interaction is also observed for $[Cd(His)-H]^+$ and $[CdCl(His)]^+$, except the carboxylic acid is deprotonated and there is no spectator Cl^- ion in the former. Structural assignment turned to be more complicated when the metal is surrounded by two amino acids. In a recent study[24], the structure of the computed ground state of $[Cd(His)(His-H)]^+$ indeed differed according to the theoretical methods used, due to very small relative energies between structures involving either a zwitterionic or a canonical intact histidine. IRMPD data tend to suggest a mixture of the two forms.

Metal ions play different roles in nucleic acids systems depending on the type of the metals.[38, 39] While alkali metals often bind to phosphate groups to DNA and RNA strands, transition-metal ions predominantly interact directly with nucleobases, and the following affinity order holds for the nucleic acid monomers: N7(guanosine) > N3-(cytidine) > N7(adenosine) > N1(adenosine) > N3(adenosine, guanosine).[40, 41] We have also mentioned the particular affinity of Hg^{2+} to the T-T pair (*vide infra*). Cadmium has been classified as a category 1 human carcinogen and cadmium-induced carcinogenicity can involve direct interaction of cadmium with DNA.[42] This has motivated different

fundamental studies about the interaction of Cd with different DNA building blocks, and notably nucleobases. In a computational study, Burda and co-workers aimed at characterizing the binding characteristics of a series of divalent metal ions (including Cd^{2+}) towards canonical forms of adenine (A) and guanine (G), [43] by considering planar *Cs* structures of the M^{2+}/nucleobase complexes, with metal cations interacting with the nitrogen N7 of adenine and N7 and O6 of guanine.

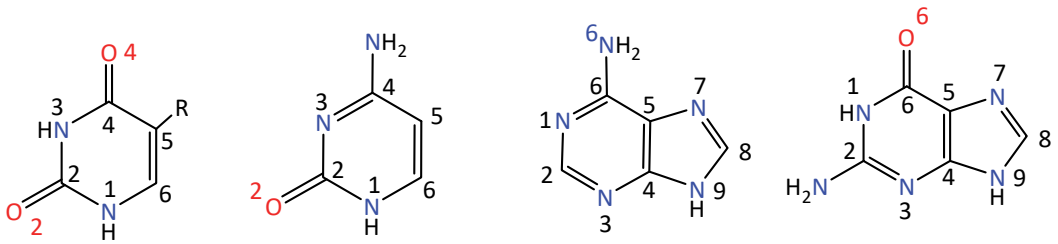

R=H : uracile
R=CH_3 : thymine

cytosine

adenine

guanine

All the intermolecular M-N7 distances for adenine-containing complexes were found shorter than the corresponding distances in guanine, due to the fact that the interaction is monodentate for the former and bidentate for the latter. The binding energy of G turned to be systematically larger than that of A, regardless the metallic center, with values estimated at -197 and -124 kcal/mol for Cd^{2+} at the MP2 level (including BSSE corrections). Later, Wu and co-workers reinvestigated the interactions of Cd^{2+} with adenine by considering different tautomeric forms.[44] Their DFT study (B3LYP) showed that the prevailing structure was not the canonical form but involved an imino tautomer with interaction of the metal with both N7 and N6 nitrogen atoms. Similarly, the most stable structure of the Cd^{2+}/thymine (T) complex also involved a keto-enol tautomeric form of T. To account for the influence of solution environment, they also performed PCM calculations, which resulted in a significant decrease in the relative energies between the different structures and a change of the global minimum. The interaction with the five nucleobases were also investigated by Bachi and co-workers.[45] Their B3LYP results are in agreement with those of Wu and co-workers concerning the Cd^{2+}/nucleobase complexes: a bidentate interaction with a tautomeric form of U, T and A, and with a canonical form of G and C. Using the global minimum for each nucleobase resulted in the following order of metal ion affinity for Cd: A>G>T>U>C. This order slightly changes when considering only canonical forms (C>G>A>T>U). Effects of Cd complexation onto the Watson-Crick base pair stability has also been investigated, by

considering interaction of the dication with only the purine bases (with nitrogen N7 of adenine in the AT pair and with nitrogen N7 and oxygen O6 of guanine in the GC pair).[43] The presence of the metal induces a significant perturbation of the Hydrogen bond network between the base pairs, Cd^{2+} and Hg^{2+} having a similar effect. The pyrimidine base turned to have a negligible effect onto the metal/purine complex, but it was observed that the stabilization energy resulting from the metal/purine base interaction was reduced when the nucleobase was engaged in the base pair. The interaction with the purine is significantly reduced when the metal is hydrated.[46] Complexes in which cadmium directly interacts with two nucleobases have also been studied, both theoretically[44] and experimentally.[47, 48] Fridgen and co-workers studied different $[M(uracil\text{-}H)(uracil)]^+$ complexes (M=Zn, Cu, Ni, Co, Fe, Mn, Cd, Pd, Mg, Ca, Sr, Ba, or Pb) by combining SORI-CID (Sustained-Off Resonance Irradiation) and IRMPD to DFT calculations.[47] These complexes could be divided into two families depending on whether they dissociate according to loss of intact uracil or HNCO (which involved C2 and N3 atoms). Regardless the metal ion, the most stable computed structure involves a metal ion ligated by N3 and O4 of deprotonated uracil and by N3 and O2 of intact uracil in its O4H tautomeric form. The differences in the observed fragmentations for the $[M(Ura{-}H)(Ura)]^+$ complexes when M=Zn, Cu, Ni, Fe, Cd, Pd, Ca, and Mg on one hand and when M=Sr, Ba, and Pb on the other hand can be explained, in part by the computed binding energies between uracil and $[M(Ura\text{-}H)]^+$, loss of intact uracil being observed for metals having the lowest binding energies (Sr, Ba and Pb). It was also found that the computed binding energies between uracil and the$[M(Ura\text{-}H)]^+$ ions globally increased as the ionic radius decreased. This group also performed IRMPD experiments on the ammoniated complexes $[[M(Ura{-}H)(Ura)NH_3]^+$.[48] The spectra of the Fe, Co, Ni, Zn, and Cd complexes are all strikingly similar and are consistent with an ammonia molecule coordinated to the metal.

To complete this bibliographic compilation, deliberately focused on the interactions of cadmium with compounds of biological interests, other gas-phase studies published recently could also be mentioned. Some provided new insights about the effect of cadmium exposure onto the plant metabolome[49, 50] or antibiotics.[51] Given the high toxicity of cadmium, many efforts are also devoted to the design of new chelates for sensitive and selective detection of Cd at low concentration and in this context, different fundamental studies about the interactions of Cd^{2+} with different mono or multidentate organic ligands were reported.[52-60] Finally, one may also mention a very nice series of studies unveiling unexpected reactions of Group IIb metal ions.[61-64]

Hg

Probably one of the first studies of the biochemical role of Hg was done by Katz in 1952, who observed that mercury chloride was able to react with salts of nucleic acids leading to a decrease in the viscosity.[65] In following years more papers were published on the peculiarities of the interaction between Hg^{2+} and DNA,[66] finding that the reaction could be reversed by adding complexing agents for Hg^{II}. A decade after the first paper aforementioned, Katz went a step further in the binding mechanism of Hg^{II} ions with polynucleotides, concluding that in the interaction with the T-T base pair Hg^{II} was coordinated to both N3 positions of the two thymine residues.[67] Later on the crystal and molecular structure of a 2:1 complex of 1-methylthymine-Hg^{II} would be reported,[68] showing that the structure was stabilized indeed by a N-Hg-N bond linking the two thymine moieties together.

We needed to wait to the first years of the 21st century to witness a significant activation of the research on the interactions between Hg^{II} and DNA, strongly motivated by the high toxicity of this metal and by the necessity of finding strategies able to detect mercury ions in the environment. As a first significant result, in 2004 it was found that the binding of Hg^{II} ions to thymine-thymine (T–T) base pairs was not only strong but also highly selective in clear contrast with other transition metal ions, such as Cu^{2+}, Ni^{2+}, Pd^{2+}, Co^{2+}, Mn^{2+}, Zn^{2+}, Pb^{2+}, Cd^{2+}, Mg^{2+}, Ca^{2+}, Fe^{2+} and Ru^{2+} that do not affect in a significant manner duplex stability.[69] Thus, the possibility of generating selective sensors for Hg^{2+} was really high through its interaction with T-T pairs. Little later, new experimental results would confirm that the stabilizing effect of Hg^{2+} on the T-T base pair surpasses the effects of other metals and seems to be highly specific.[70] A posterior analysis of ^{15}N-^{15}N J-coupling across Hg^{II} provided a direct evidence for the formation of T-Hg^{II}-T pairs. These conclusions were coherent with the results obtained through the use of electrospray ionization mass spectrometry (ESI-MS), fluorescence and circular dichroism (CD) spectroscopy.[71] It was also found that the T–Hg^{II}–T base pair plays a role in the biochemistry of polymerases opening new possibilities for the metal-ion-mediated enzymatic incorporation of a variety of artificial bases into oligonucleotides.[72] Rather interestingly it was also reported that the thermal stability of the duplex DNA with the T-Hg-T base pair is comparable to that of the corresponding T:A or A:T base pairs.[73] In the same paper the binding constant for the specific binding of Hg^{2+} to a T:T mismatch was reported.[73] Also, new ESI-MS/MS studies on selected oligodeoxynucleotides rich and

poor in thymine indicated that Hg^{II} prefers thymines over the other binding sites in oligonucleotides both in solution and in the gas phase.[74] An interesting computational study[75] along with the experimental data reported by Miyake et al.[70] mentioned above, provided a very interesting information on the structural properties, electronic structure and UV absorption spectra of the (T–Hg^{II}–T) base pair, showing not only the nature of the Hg-N bonding but also that the metal–metal interaction between two Hg^{II} in multiple stacking T–Hg^{II}–T is the origin of the significant changes in the UV absorption spectra. Similar results were obtained by means of electrospray ionization-tandem mass spectrometry.[76] The role of metal-base pairs in DNA-like materials with a superior conductivity and their use for new nano-electronic applications was analyzed in this period too.[77]

Ono et al.[78] reported the synthesis of covalently linked parallel and antiparallel DNA duplexes containing the metal-mediated base pairs T–Hg^{II}–T, and an interesting review on the binding of metal ions by pyrimidine base pairs in DNA duplexes.[79] Later on, new perspectives on the incorporation of Hg^{2+} into DNA Duplex,[80] on the role of Hg^{2+} in the stability of duplexes with non-canonical dU–dU pairs,[81] on the expansion of the concept to metal-mediated base triples and base tetrads,[82] and on its effects on the thermal stabilities of DNA duplexes containing homo- and heterochiral mismatched base pairs,[83] would be also reported.

Specific studies in this field were devoted to DNA damage[84-86] induced by Hg^{II}, to the role of Hg^{2+} on the construction of DNA molecular logic gates that produce electrochemiluminescent signals,[87] and to the photoluminescent properties of phenylmercury(II) complexes.[88]

In relation to the formation of the T-Hg^{II}-T base pairs, is particularly important the role played by the so-called nucleophilic attraction.[89] This phenomenon , as pointed out by Benda et al.,[90] is behind the stabilizing effect that $Hg^{II}\cdots Hg^{II}$ non-covalent interactions between the consecutive Hg^{II}-mediated base pairs have on the nucleic acid structures. Subsequent studies by Raman spectroscopy[91] and theoretical calculations[92] would confirm these first conclusions. More recently, Hg^{II} was also found to bind C-T mismatches with high affinity,[93] and that the formation of these Hg^{II}-mediated base pairs can be triggered by irradiation with light.[94] The three-dimensional structure of metallo-DNA with consecutive T–Hg^{II}–T base pairs also confirm the critical role of the $Hg^{II}\cdots Hg^{II}$ non-covalent interactions in the stabilization of the 3D building, explaining at the same time the positive entropy for the metallo-base pair formation.[95] Along these

lines, the first crystal structure reported for a DNA duplex containing two consecutive T–Hg^{II}–T base pairs showed structural features, such as N3-Hg and Hg^{II}-Hg^{II} distances fully compatible with the previous studies on these systems, suggesting that the metallophilic attraction could certainly stabilize the B-form of the double helix.[96] Results obtained from DFT calculations on $(T\text{-}Hg\text{-}T)_3$ and $(U\text{-}Hg\text{-}U)_3$ were consistent[97] with these experimental observations. Little later, the first determination of the one-bond $^1J(^{199}Hg,^{15}N)$ coupling characterizing the unique physicochemical properties of the N–Hg^{II} interactions in T-Hg^{II}-T systems, was reported.[98] Although, to the best of our knowledge, the first fluorescence study on T–Hg^{II}–T base pairs was reported in 2008,[99] the most complete characterization of the fluorescence of this system would be reported eight years later through the use of the thymidine analogue ^{DMA}T that exhibits the same base pairing preferences as native thymine residues.[100] In this way, it was possible to show that the fluorescence properties of ^{DMA}T-A base pairs reflected the exceptionally high kinetic stability of T-Hg^{II}-T base pairs and that they could have a high potential to disrupt DNA metabolism in vivo.[100] Later on, highly sensitive fluorometric methods for the determination of Hg^{II} ions were described.[101] A study of the interactions of Hg^{II} with T-T mispair containing hairpin loops, including UV-visible thermal circular dichroism analyses,[102] demonstrated that the number of T-T mispairs in oligonucleotide probes plays an important role for Hg (II) binding, presumably due to an increase in cooperative binding.

One very interesting application of metal-mediated base pairs is their use as metal-ion sensors.[103] This is particularly the case when dealing with T-Hg^{2+}-T base pairs,[104] due to the high toxicity of Hg^{2+} cations. Also, the fact that Hg^{2+} is capable of forming T-Hg-T base pairs and that Hg^{2+} can be reduced to $(Hg_2)^{2+}$ was the base to generate fluorescence sensors.[105] Similarly, the stabilization of T:T mismatches by Hg^{2+} ions, may be used for the detection of single nucleotide polymorphisms.[104] Also, voltammetric[106] new electrochemical DNA-based biosensors based on blue modified electrodes[107] and on ligase mediated creation of G-quadruplex-hemin DNAzyme[108] were designed for the selective determination of the Hg_2. Interesting are the applications in generating DNA nanomachines.[109] Other potential uses have been described in some interesting feature articles.[110, 111]

Although most of the publications compiled in the previous paragraphs were focused on the interaction of different forms of mercury with thymine, some attention was also paid to the interactions with other biochemical bases. As suitable examples the

theoretical study of the interactions of cysteine with Cu^{2+}, Zn^{2+}, Cd^{2+} and Hg^{2+} using DFT calculations, [7] the experimental and theoretical investigation of the photophysics and photochemistry of Hg^{2+} with mono- and bisporphyrins,[112] the binding of Hg^{2+} with cysteine, dipeptide Cys-Gly and reduced glutathione by electrospray ionization mass-spectrometry and isothermal titration calorimetry,[113] the design of new methods for removal of Hg(II), based on the appealing interaction between Hg^{2+}, exfoliated graphene oxide (EGO) and L-cystine,[114] or the investigation of the properties of 5-mercurycytosine, [115] should be mentioned.

In any overview on the biochemistry of mercury, it is necessary to remember that this element can be present not only as Hg^{2+} but in other chemical forms. Among them, methylmercury (CH_3Hg^+) has received also much attention, because, due to its high liposolubility which allows it to easily pass through the cell membranes, becomes one of the most toxic forms of mercury.[116] On the other hand, though it is a much softer acid than the proton, CH_3Hg^+ reacts strongly with aminoacids[117] and shows an extremely high affinity for cystine and polypeptide residues.[118] The sequestering ability of some S, N, and O donor ligands towards CH_3Hg^+ was evaluated showing that all S donor ligands show a good sequestering power.[119] In our group we have also investigated the gas-phase interactions of uracil and thymine with alkylmercury cations, in particular CH_3Hg^+, n-$BuHg^+$ and t-$BuHg^+$ in a combined experimental and theoretical approach.[120] A combination of electrospray ionization coupled to tandem mass spectrometry Infrared Multiple Photon Dissociation (IRMPD) techniques and DFT calculations allowed us to conclude that the aforementioned ions exhibit a peculiar reactivity characterized by the transfer of the alkyl group to the nucleobases, the dominant reaction being the alkylation of the nucleobase, $[R(NB)]^+$ with the concomitant loss of neutral Hg.[120]

We have cited in previous paragraphs papers in which different experimental techniques were nicely complemented by different computational approaches to address structural and bonding questions related with complexes involving Hg. Here, we will pay attention to studies done exclusively on theoretical grounds with the aim of improving the knowledge on the structural and bonding characteristics of the complexes between Hg^{2+} and CH_3Hg^+ and different biochemical systems. Although no biochemical systems are involved, our first citation should correspond to the Filatov and Cremer's pioneering work on the bonding of mercury chalcogenides,[121] because it contributes significantly to understand the bonding characteristics of an element for which this information is extremely scarce. Indeed, very few theoretical studies on the bonding between

biochemical systems and Hg can be reported. Among them, the Hg binding to biothiols[122] or to flurbiprofen,[123] the complexes of Hg^{II} with sulfur- and aminopyridine-containing chelating resins,[124] and the interaction of Hg^{2+} cations with the most stable tautomeric forms of free DNA and RNA bases,[45] should be reported. To finish this compilation, the paper on spodium bonds, which refer to a net attractive interaction between any element of Group 12 (Zn,Cd, Hg) and electron-rich atoms should be cited because it provides a bonding analysis that can be useful to understand the structure and stability of biochemical systems interacting with these three metals.[125]

Pb

Lead is a normal constituent of the earth's crust (approx. 20 ppm), with trace amounts found naturally in soil, plants, and water. Lead, probably before the Bronze or Iron Ages, was used in some cultures in medicine and cosmetics (*kohl*) because of abundance and ease in obtaining it. Due to anthropogenic activities, lead is commonly found in our groundwater and accumulated in waste, but its use is likely to be rare in modern age because the lead toxicity is well known, as long-term exposure or inhalation of lead can cause death. Since its dangerousness is very high many studies are already underway to eliminate it using different inorganic molecules,[126] of which superchalchogens are a good recent example.[127] Not surprisingly there is a particular interest on its effects in biological homeostasis,[128] and consequently many studies in the literature have focused their attention on the specific toxic effects on human health.[129-131] These harmful effects usually affect major organs including liver, heart and kidneys.[128, 132] Lead can be in an ionic form or as an oxide, but both are toxic though the former is more reactive and interacts more easily with organic molecules. Indeed the number of chemical reactions in which it can participate, probably due to a high affinity for proteins forming bioaccumulative harmful adducts in the human body is very large.[133] The first evidence was reported as early as 1952, by Klotz et al.[134] on the absorption spectra on [Pb(II)] binding to proteins adducts.

To review recent studies on molecules interacting with lead, it is reasonable to remember that this metal tends to easily associate with electron donors such as oxygen, nitrogen and sulfur.[135, 136] In molecules similar to porphyrin, lead as a dication is usually bound to nitrogen atoms through a dative bond. Recent synthesis, characterization and computational studies of tetraacetamide derivatives of tetraazacycloalkane as ligand with this metal show this type of bonding.[137] The *peri*-substituted naphthalene and bis(5-

(pyrazin-2-yl)-1,2,4-triazol-3-yl) methane interaction with Pb(II) also evidence such an association.[138, 139] If one replaces nitrogen with an oxygen atom, one can find crown ether derivatives that also have electronic pairs available in their central atoms. Nevertheless, the crown cavity is smaller than the metal size which leads to metal sandwich complexes formation, and the interaction can be found with both the monocation and the dication. A study performed by Franski using collision-induced dissociation tandem mass spectrometry showed how singly charged sandwich complexes between ether crown and lead can be easily formed after removing a hydrogen atom.[60] At the same time, doubly charged sandwich complexes have also been detected but they were difficult to generate experimentally.[60] In addition to interactions in which the cavity is formed only by nitrogen or oxygen, cases in which the cavity involves both atoms have also been studied. This is the case of the interaction of ethylenediaminetetraacetic acid (EDTA) anions (i.e. $[EDTA\text{-}nH]^{n-}$, n=1–4) with Pb(II) where the metal could coordinate with two nitrogens and two or even 4 oxygen atoms.[140] This process is followed, as revealed by mass spectrometry,[140] by removal from the ligand up to a maximum of 4 protons, leaving a complex where lead is hexacoordinated,[140] though other fragmentation observed involves the loss of CO_2. Due to the easy deprotonation of aminoacids when interacting with Pb^{2+}, most of the studies deal with the resulting monocations. The most recent publication on this topic deals with the interaction between L-proline and Pb^{2+} where $[Pb(Pro\text{-}H)]^+$ complexes are characterized at the X3LYP and M06-L levels of theory.[141] Likely, the most extensive study dealing with amino acids was reported by Fridgen et al.[142] and dates back to a decade ago. In this study eight $[Pb\text{-}(amino\ acid\text{-}H)H_2O)]^+$ complexes have been explored by blackbody infrared radiative dissociation (BIRD) and computational formalisms. The amino acids explored were Gly, Ala, Val, Leu, Ile, Phe, Glu, and Lys which have shown that there is a link between their gas-phase basicities and the ability of resulting deprotonated species $[Pb(amino\ acid\text{-}H)]^+$ to attach water, since amino acids with stronger basicities donate more electron density to Pb^{2+} and weaken its bond with the water oxygen. The values of the binding energies with water induced by the presence of lead estimated at the B3LYP level range from 77 to 114 kJ/mol^{-1}. Consistently, the same year Bohme et al.[143] published a study of 15 deprotonated amino acids after interacting with lead(II). In this case the lead dication and complexes were electro-sprayed from solution and subjected to collision-induced dissociation in a tandem mass spectrometer. The C-αC bond of the amino acid was found to be activated by Pb^{2+} by the same mechanism that influences the gas-phase acidities of the amino acids. Bond

activation by Pb^{2+} appears to be the largest with deprotonated glycine[144, 145] and is also large with the other deprotonated amino acids containing hydrocarbon side chains (alanine, proline and valine). Later on, an IRMPD spectroscopy study together with computational analyses were carried out to determine the structures of deprotonated Phenylalanine and Glutamic acid with Pb(II).[146] It was shown, both on experimental and theoretical grounds, that the proton is removed from the carboxylic group whereas the metal bidentates between the amino group and the carbonyl of the amino acid, and that the interaction of water in $[Pb(Phe\text{-}H)H_2O)]^+$ and $[Pb(Glu\text{-}H)H_2O]^+$ gives rise to a tetracoordinated lead structure in the gas phase.

Although our objective is to discuss the interactions of lead with different molecules of biological interest, and not to discuss and analyze the different types of lead coordination, this analysis can be found in the review published by Aboutorabi et al.[147]

Concerning the interaction of nucleobases with lead, the first reported study was focused on uracil and thymine.[148, 149] The presence of two different carbonyl types and the deprotonation induced by Pb^{2+} were explored by means of mass spectrometry and theoretical calculations. The metal interacts preferentially with the oxygen at position 4 after removing the hydrogen ligated to the nitrogen at position 3. Also, the cleavage of the most important fragments (PbNCO and HNCO) was elucidated. Similar conclusions were reported for thiouracil derivative,[150] though in this case the metal preferred interaction site is always the sulfur atom. For 2,4-dithiouracil the interaction takes place at position 4, and the deprotonation takes place from the same nitrogen atom as in uracil and thymine. In $[Pb(cytosine\text{-}H)]^+$ many patterns of lead interaction are repeated.[151] The bonding is bidentate with the carbonyl oxygen atom and the adjacent nitrogen, as confirmed by IRMPD spectra. The deprotonation involves in this case the NH group at position 1. In all the cited molecules, lead activates the cleavage of C1-N3 bond to eliminate HNCO. If we switch to the deprotonated dimer of uracil with lead, $[Pb(Ura\text{-}H)Ura]^+$, the interaction is tetradentate involving the same active sites as above.[152] The deprotonation is at the same site and the metal binds to two nitrogen and two oxygen atoms, because an internal hydrogen transfer is observed involving the NH group of the other monomer. The loss of HNCO in this case is not observed but the departure of an uracil molecule occurs instead.[153] It is worth noting that this study was done recovering the interaction of deprotonation of uracil dimer with other heavy metals such as Zn, Cu, Ni, Co, Fe, Mn, Cd, Pd , Mg, Ca, Sr, and Ba (see also Cd section, *vide supra*).

As far as we know the reactivity of the complexes between adenine and guanine and lead was not explored. On the other hand, complexes generated in the gas phase between Pb^{2+} and deprotonated 2'-deoxyguanosine-5'-monophosphate (dGMP), 2'-deoxycytidine-5'-monophosphate (dCMP), cytidine-5'-monophosphate (CMP) and uridine-5'-monophosphate (UMP) were studied both computationally and by IRMPD spectroscopy.[154-156] All these complexes are found to be macrochelates, involving simultaneous interaction of the metal with the deprotonated phosphate group and the nucleobase moiety. Remarkably, in the particular case of UMP, the binding scheme involves a tautomeric form of uracil.[155]

References

1. A. Hartwig, *Antioxid. Redox Signal.*, 2001, **3**, 625-634.
2. C. T. McMurray and J. A. Tainer, *Nat. Genet.*, 2003, **34**, 239-241.
3. G. W. Buchko, N. J. Hess and M. A. Kennedy, *Carcinogenesis*, 2000, **21**, 1051-1057.
4. M. J. Stillman, *Coord. Chem. Rev.*, 1995, **144**, 461-511.
5. C. D. Klaassen, J. Liu and S. Choudhuri, *Annu. Rev. Pharmacol. Toxicol.*, 1999, **39**, 267-294.
6. J. W. Ejnik, A. Munoz, E. DeRose, C. F. Shaw and D. H. Petering, *Biochemistry*, 2003, **42**, 8403-8410.
7. M. Belcastro, T. Marino, N. Russo and M. Toscano, *J. Mass Spectrom.*, 2005, **40**, 300-306.
8. P. B. Armentrout, E. I. Armentrout, A. A. Clark, T. E. Cooper, E. M. S. Stennett and D. R. Carl, *J. Phys. Chem. B*, 2010, **114**, 3927-3937.
9. M. Citir, E. M. S. Stennett, J. Oomens, J. D. Steill, M. T. Rodgers and P. B. Armentrout, *Int. J. Mass Spectrom.*, 2010, **297**, 9-17.
10. S. Mori, T. Endoh, Y. Yaguchi, Y. Shimizu, T. Kishi and T. K. Yanai, *Theo. Chem. Acc.*, 2011, **130**, 279-297.
11. F. Rogalewicz, Y. Hoppilliard and G. Ohanessian, *Int. J. Mass Spectrom.*, 2000, **201**, 307-320.
12. F. Rogalewicz, Y. Hoppilliard and G. Ohanessian, *Int. J. Mass Spectrom.*, 2001, **206**, 45-52.
13. F. Rogalewicz, Y. Hoppilliard and G. Ohanessian, *Int. J. Mass Spectrom.*, 2003, **227**, 439-451.
14. N. Burford, M. D. Eelman and W. G. LeBlanc, *Can. J. Chem.*, 2004, **82**, 1254-1259.
15. T. E. Hofstetter, C. Howder, G. Berden, J. Oomens and P. B. Armentrout, *J. Phys. Chem. B*, 2011, **115**, 12648-12661.
16. R. A. Coates, C. P. McNary, G. C. Boles, G. Berden, J. Oomens and P. B. Armentrout, *Phys. Chem. Chem. Phys.*, 2015, **17**, 25799-25808.
17. G. C. Boles, R. A. Coates, G. Berden, J. Oomens and P. B. Armentrout, *J. Phys. Chem. B*, 2016, **120**, 12486-12500.

18. R. A. Coates, G. C. Boles, C. P. McNary, G. Berden, J. Oomens and P. B. Armentrout, *Phys. Chem. Chem. Phys.*, 2016, **18**, 22434-22445.
19. G. C. Boles, C. J. Owen, G. Berden, J. Oomens and P. B. Armentrout, *Phys. Chem. Chem. Phys.*, 2017, **19**, 12394-12406.
20. G. C. Boles, R. L. Hightower, R. A. Coates, C. P. McNary, G. Berden, J. Oomens and P. B. Armentrout, *J. Phys. Chem. B*, 2018, **122**, 3836-3853.
21. A. M. Chalifoux, G. C. Boles, G. Berden, J. Oomens and P. B. Armentrout, *Phys. Chem. Chem. Phys.*, 2018, **20**, 20712-20725.
22. G. C. Boles, R. L. Hightower, G. Berden, J. Oomens and P. B. Armentrout, *J. Phys. Chem. B.*, 2019, **123**, 9343-9354.
23. C. J. Owen, G. C. Boles, G. Berden, J. Oomens and P. B. Armentrout, *Eur. J. Mass Spectom.*, 2019, **25**, 97-111.
24. B. C. Stevenson, J. Martens, G. Berden, J. Oomens, M. Schaefer and P. B. Armentrout, *J. Phys. Chem. A*, 2020, **124**, 10266-10276.
25. G. C. Boles, B. C. Stevenson, R. L. Hightower, G. Berden, J. Oomens and P. B. Armentrout, *J. Mass. Spect.*, 2021, **56**.
26. N. Burford, M. D. Eelman and K. Groom, *J. Inorg. Biochem.*, 2005, **99**, 1992-1997.
27. F. M. Rubino, M. Pitton, G. Brambilla and A. Colombi, *J. Am. Soc. Mass Spectrom.*, 2006, **17**, 1442-1455.
28. F. M. Rubino, C. Verduci, R. Giampiccolo, S. Pulvirenti, G. Brambilla and A. Colombi, *J. Am. Soc. Mass Spectrom.*, 2004, **15**, 288-300.
29. L. Rulisek and Z. Havlas, *J. Am. Chem. Soc.*, 2000, **122**, 10428-10439.
30. E. Ahlstrand, D. Spangberg, K. Hermansson and R. Friedman, *Int. J. Quant. Chem.*, 2013, **113**, 2554-2562.
31. L. MacAleese and P. Maitre, *Mass Spectom. Rev.*, 2007, **26**, 583-605.
32. T. D. Fridgen, *Mass. Spectom. Rev.*, 2009, **28**, 586-607.
33. N. C. Polfer and J. Oomens, *Mass. Spectrom. Rev.*, 2009, **28**, 468-494.
34. J. S. Brodbelt, *Chem. Soc. Rev.*, 2014, **43**, 2757-2783.
35. P. B. Armentrout, Y. Chen and M. T. Rodgers, *J. Phys. Chem. A.*, 2012, **116**, 3989-3999.
36. G. C. Boles, R. A. Coates, G. Berden, J. Oomens and P. B. Armentrout, *J. Phys. Chem. B*, 2015, **119**, 11607-11617.
37. R. A. Coates, C. P. McNary, G. C. Boles, G. Berden, J. Oomens and P. B. Armentrout, *Phys. Chem. Chem. Phys.*, 2017, **19**, 18777-18778.
38. B. Lippert, *Coord. Chem. Rev.*, 2000, **200**, 487-516.
39. M. Noguera, V. Branchadell, E. Constantino, R. Rios-Font, M. Sodupe and L. Rodriguez-Santiago, *J. Phys. Chem. A*, 2007, **111**, 9823-9829.
40. R. B. Martin, *Acc. Chem. Res.*, 1985, **18**, 32-38.
41. H. Sigel, *Chem. Soc. Rev.*, 1993, **22**, 255-267.
42. T. P. Coogan, R. M. Bare and M. P. Waalkes, *Toxicol. Appl. Pharmacol.*, 1992, **113**, 227-233.
43. J. V. Burda, J. Sponer, J. Leszczynski and P. Hobza, *J. Phys. Chem. B*, 1997, **101**, 9670-9677.
44. Y. Wu, R. Sa, Q. Li, Y. Wei and K. Wu, *Chem. Phys. Lett.* , 2009, **467**, 387-392.
45. S. Bagchi, D. Mandal, D. Ghosh and A. K. Das, *Chem. Phys.*, 2012, **400**, 108-117.
46. J. Sponer, J. V. Burda, M. Sabat, J. Leszczynski and P. Hobza, *J. Phys. Chem. A*, 1998, **102**, 5951-5957.

47. O. Y. Ali, N. M. Randell and T. D. Fridgen, *ChemPhysChem*, 2012, **13**, 1507-1513.
48. B. Power, S. Rowe and T. D. Fridgen, *J. Phys. Chem. B*, 2017, **121**, 58-65.
49. J. J. Dytrtova, M. Jakl and D. Schröder, *Talanta*, 2012, **90**, 63-68.
50. M. Navarro-Reig, J. Jaumot, B. Pina, E. Moyano, M. T. Galceran and R. Tauler, *Metallomics*, 2017, **9**, 660-675.
51. R. C. Dunbar, J. Oomens, G. Orlova and D. K. Bohme, *Int. J. Mass. Spectrom.*, 2011, **308**, 330-337.
52. J. H. Elnakat, I. G. Dance, K. J. Fisher and G. D. Willett, *Polyhedron*, 1994, **13**, 409-415.
53. J. M. J. Nuutinen, J. Ratilainen, K. Rissanen and P. Vainiotalo, *J. Mass Spectrom.*, 2001, **36**, 902-910.
54. Z. H. Li, J. Liu, M. Qiao and K.-N. Fan, *Mol. Phys.*, 2009, **107**, 1271-1282.
55. T. E. Cooper, D. R. Carl, J. Oomens, J. D. Steill and P. B. Armentrout, *J. Phys. Chem. A*, 2011, **115**, 5408-5422.
56. J. Jia, Q.-C. Xu, R.-c. Li, X. Tang, Y.-F. He, M.-Y. Zhang, Y. Zhang and G.-W. Xing, *Org. Biomol. Chem.*, 2012, **10**, 6279-6286.
57. T. Sun, N. Ji, M. Qi, Z. Tao and R. Fu, *J. Chromatogr. A*, 2014, **1343**, 167-173.
58. N. J. Rijs, T. Weiske, M. Schlangen and H. Schwarz, *Anal. Chem.*, 2015, **87**, 9769-9776.
59. Z. Y. Zhang, C. F. Bi, Y. H. Fan, X. C. Yan, X. Zhang, P. F. Zhang and G. M. Huang, *Russ. J. Coord. Chem.*, 2015, **41**, 274-284.
60. R. Franski, *Rapid Comm. Mass Spectom.*, 2018, **32**, 1651-1657.
61. R. Kretschmer, M. Schlangen and H. Schwarz, *Angew. Chem., Int. Ed.*, 2011, **50**, 5387-5391.
62. R. Kretschmer, M. Schlangen, M. Kaupp and H. Schwarz, *Organometallics*, 2012, **31**, 3816-3824.
63. R. Kretschmer, M. Schlangen and H. Schwarz, *Chem. Eur. J.*, 2012, **18**, 40-49.
64. L. Yue, S. Zhou, X. Sun, M. Schlangen and H. Schwarz, *Angew. Chem. Int. Ed.*, 2018, **57**, 3251-3255.
65. S. Katz, *J. Am. Chem. Soc.* , 1952, **74**, 2238-2245.
66. T. Yamane and N. Davidson, *J. Am. Chem. Soc.*, 1962, **83**, 2599–2607.
67. S. Katz, *Nature*, 1962, **194**, 569.
68. L. D. Kosturko, C. Folzer and R. F. Stewart, *Biochemistry*, 1974, **13**, 3949–3952.
69. A. Ono and H. Togashi, *Angew. Chem.*, 2004, **116**, 4400 –4402.
70. Y. Miyake, H. Togashi, M. Tashiro, H. Yamaguchi, S. Oda, M. Kudo, Y. Tanaka, Y. Kondo, R. Sawa, T. Fujimoto, T. Machinami and A. Ono, *J. Am. Chem. Soc.*, 2006, **128**, 2172-2173.
71. C.-K. Chiang, Y.-W. Lin, C.-C. Hu and H.-T. Changa, *J. Am. Soc. Mass Spectrom.*, 2009, **20**, 1834–1840.
72. H. Urata, E. Yamaguchi, T. Funai, Y. Matsumura and S.-i. Wada, *Angew. Chem. Int. Ed.*, 2010, **49**, 6516-6519.
73. H. Torigoe, A. Ono and T. Kozasa, *Chem. Eur. J.*, 2010, **16**, 13218-13225.
74. J. Anichina, Z. Dobrusin and D. K. Bohme, *J. Phys. Chem. B*, 2010, **114**, 15106-15112.
75. H. Miyachi, T. Matsui, Y. Shigeta and K. Hirao, *Phys. Chem. Chem. Phys.*, 2010, **12**, 909–917.
76. R. Zhang, X. Zhuang, S. Liu, F. Song and Z. Liu, *Anal. Methods*, 2014, **6**, 5746-5752.
77. G. H. Clever and M. Shionoya, *Coord. Chem. Rev.*, 2010, **254**, 2391-2402.

78. T. Ono, K. Yoshida, Y. Saotome, R. Sakabe, I. Okamoto and A. Ono, *Chem. Comm.*, 2011, **47**, 1542-1544.
79. A. Ono, H. Torigoe, Y. Tanaka and I. Okamoto, *Chem. Soc. Rev.*, 2011, **40**, 5855-5866.
80. B. Jash and J. Mueller, *Chem. Eur. J.*, 2018, **24**, 10636-10640.
81. X. Guo, S. A. Ingale, H. Yang, Y. He and F. Seela, *Org. Biomol. Chem.*, 2017, **15**, 870-883.
82. S. Naskar, R. Guha and J. Mueller, *Angew. Chem. Int. Ed.*, 2020, **59**, 1397-1406.
83. T. Funai, N. Adachi, M. Aotani, S.-i. Wada and H. Urata, *Nucleosides Nucleotides & Nucleic Acids*, 2020, **39**, 310-321.
84. M. B. Halli and R. B. Sumathi, *J. Mol. Struct.*, 2012, **1022**, 130-138.
85. T. Zhang, Q. Lu, C. Su, Y. Yang, D. Hu and Q. Xu, *Ecotoxicol. Environ. Saf.*, 2017, **143**, 46-56.
86. S. Roos-Muñoz, D. Voltolina, M. Aguilar-Juárez, S. Abad-Rosales, J. C. Bautista-Covarrubias, M. Isaura Banuelos-Vargas, M. F. Soto-Jiménez and M. G. Frías-Espericueta, *Bull. Environ. Contam. Toxic.*, 2019, **102**, 186-190.
87. X. Li, L. Sun and T. Ding, *Biosens. Bioelectron.*, 2011, **26**, 3570-3576.
88. A. Bharti, P. Bharati, R. Dulare, M. K. Bharty, D. K. Singh and N. K. Singh, *Polyhedron*, 2013, **65**, 170-180.
89. P. Pyykkö, *Chem. Rev.*, 1997, **97**, 597–636.
90. L. Benda, M. Straka, Y. Tanaka and V. Sychrovsky, *Phys. Chem. Chem. Phys.*, 2011, **13**, 100-103.
91. T. Uchiyama, T. Miura, H. Takeuchi, T. Dairaku, T. Komuro, T. Kawamura, Y. Kondo, L. Benda, V. Sychrovsky, P. Bour, I. Okamoto, A. Ono and Y. Tanaka, *Nucleic Acids Res.*, 2012, **40**, 5766-5774.
92. L. Benda, M. Straka, V. Sychrovsky, P. Bour and Y. Tanaka, *J. Phys. Chem. A*, 2012, **116**, 8313-8320.
93. O. P. Schmidt, A. S. Benz, G. Mata and N. W. Luedtke, *Nucleic Acids Res.*, 2018, **46**, 6470-6479.
94. S. Naskar and J. Mueller, *Chem. Eur. J.*, 2019.
95. H. Yamaguchi, J. Sebera, J. Kondo, S. Oda, T. Komuro, T. Kawamura, T. Dairaku, Y. Kondo, I. Okamoto, A. Ono, J. V. Burda, C. Kojima, V. Sychrovsky and Y. Tanaka, *Nucleic Acids Res.*, 2014, **42**, 4094-4099.
96. J. Kondo, T. Yamada, C. Hirose, I. Okamoto, Y. Tanaka and A. Ono, *Angew. Chem. Int. Ed.*, 2014, **53**, 2385-2388.
97. T. Marino, *J. Mol. Mod.*, 2014, **20**.
98. T. Dairaku, K. Furuita, H. Sato, J. Sebera, D. Yamanaka, H. Otaki, S. Kikkawa, Y. Kondo, R. Katahira, F. M. Bickelhaupt, C. F. Guerra, A. Ono, V. Sychrovsky, C. Kojima and Y. Tanaka, *Chem. Comm.*, 2015, **51**, 8488-8491.
99. X. Xue, F. Wang and X. Liu, *J. Am. Chem. Soc.*, 2008, **130**, 3244-3245.
100. O. P. Schmidt, G. Mata and N. W. Luedtke, *J. Am. Chem. Soc.*, 2016, **138**, 14733-14739.
101. Z. Zhang, F. Zhang, P. He, X. Zhang and W. Song, *Microchimica Acta*, 2019, **186**.
102. A. Kamal, Z. She, R. Sharma and H.-B. Kraatz, *Electrochimica Acta*, 2017, **243**, 44-52.
103. X.-B. Zhang, R.-M. Kong and Y. Lu, *Annu. Rev. Anal. Chem.*, 2011, **4**, 105-128.
104. P. Scharf and J. Miller, *ChemPlusChem* 2013, **78**, 20-34.
105. Y. Miyake and A. Ono, *Tetrahedron Lett.*, 2005, **46**, 2441-2443.
106. A. Kowalczyk and A. M. Nowicka, *Sens. Actuators B Chem.*, 2016, **237**, 810-816.

107. C. Tortolini, P. Bollella, M. L. Antonelli, R. Antiochia, F. Mazzei and G. Favero, *Biosens. Bioelectron.*, 2015, **67**, 524-531.
108. G. Li, Z. Li, X. You, J. Chen and S. Tang, *Talanta*, 2016, **161**, 138-142.
109. K.-T. Liu and S.-Y. Ran, *Phys. Chem. Chem. Phys.*, 2019, **21**, 2919-2928.
110. Y. Tanaka, J. Kondo, V. Sychrovsky, J. Sebera, T. Dairaku, H. Saneyoshi, H. Urata, H. Torigoe and A. Ono, *Chem. Comm.*, 2015, **51**, 17343-17360.
111. A. Ono, H. Kanazawa, H. Ito, M. Goto, K. Nakamura, H. Saneyoshi and J. Kondo, *Angew. Chem. Int. Ed.*, 2019, **58**, 16835-16838.
112. Z. Valicsek, G. Lendvay and O. Horváth, *J. Phys. Chem. B*, 2008, **112**, 14509–14524.
113. E. Chekmeneva, J. Manuel Diaz-Cruz, C. Arino and M. Esteban, *J. Electroanal. Chem.*, 2010, **644**, 20-24.
114. A. S. K. Kumar and S.-J. Jiang, *RSC Adv.*, 2015, **5**, 6294-6304.
115. D. Ukale, V. S. Shinde and T. Lonnberg, *Chem. Eur. J.*, 2016, **22**, 7917-7923.
116. J. P. K. Rooney, *Toxicology*, 2007, **234**, 145-156.
117. A. J. Canty, R. Colton, A. Dagostino and J. C. Traeger, *Inorg. Chim. Acta*, 1994, **223**, 103-107.
118. A. DAgostino, R. Colton, J. C. Traeger and A. J. Canty, *Eur. Mass Spectrom.*, 1996, **2**, 273-285.
119. G. Falcone, C. Foti, A. Gianguzza, O. Giuffre, A. Napoli, A. Pettignano and D. Piazzese, *Anal. Bioanal. Chem.*, 2013, **405**, 881-893.
120. J.-Y. Salpin, V. Haldys, L. Latrous, J.-C. Guillemin, J. Tortajada, E. Leon, O. Mó, M. Yáñez and M. Merced Montero-Campillo, *Int. J. Mass Spectrom.*, 2019, **436**, 153-165.
121. M. Filatov and D. Cremer, *ChemPhysChem*, 2004, **5**, 1547-1557.
122. E. M. Krupp, B. F. Milne, A. Mestrot, A. A. Meharg and J. Feldmann, *Anal. Bioanal. Chem.*, 2008, **390**, 1753-1764.
123. S. Sagdinc and H. Pir, *Spectrochim. Acta*, 2009, **73**, 181-194.
124. Y. Niu, S. Feng, R. Qu, Y. Ding, D. Wang and Y. Wang, *Int. J. Quant. Chem.*, 2011, **111**, 991-1001.
125. A. Bauzà, I. Alkorta, J. Elguero, T. J. Mooibroek and A. Frontera, *Angew. Chem. Int. Ed.*, 2020, **59**, 17482 –17487.
126. T. O. Ajiboye, O. A. Oyewo and D. C. Onwudiwe, *Chemosphere*, 2021, **262**, 128379.
127. A. Omidvar, *J. Env. Chem. Eng.*, 2021, **9**, 104787.
128. R. A. Goyer, H. G. Seiler, H. Sigel and A. Sigel, *Handbook on Toxicity of Inorganic Compounds*, Dekker, New York, 1988.
129. L. S. Busenlehner, N. J. Cosper, R. A. Scott, B. P. Rosen, M. D. Wong and D. P. Giedroc, *Biochemistry*, 2001, **40**, 4426-4436.
130. J. C. Payne, M. A. ter Horst and H. A. Godwin, *J. Am. Chem. Soc.*, 1999, **121**, 6850-6855.
131. R. K. Mehra, V. R. Kodati and R. Abdullah, *Biochem. Biophys. Res. Comm.*, 1995, **215**, 730-736.
132. K. S. Egorova and V. P. Ananikov, *Organometallics*, 2017, **36**, 4071-4090.
133. A. El-Khatib, A. Hegazy and A. M. Abo-El-Kassem, *Int. J. phytoremediation*, 2014, **16**, 29-45.
134. I. M. Klotz, J. M. Urquhart and H. A. Fiess, *J. Am. Chem. Soc.*, 1952, **74**, 5537-5538.
135. M. V. M. Meuser, D. G. S. Quattrociocchi, L. M. Da Costa, G. B. Ferreira and J. W. d. M. Carneiro, *Polyhedron*, 2015, **102**, 193-200.

136. L. Puskar, P. E. Barran, B. J. Duncombe, D. Chapman and A. J. Stace, *J. Phys. Chem. A*, 2005, **109**, 273-282.
137. K. Lyczko, M. Lyczko and M. Pruszyński, *Polyhedron*, 2020, **192**, 114822.
138. M. Aman, L. Dostál, T. Mikysek, Z. Růžičková, S. Mebs, J. Beckmann and R. Jambor, *Eur. J. Inorg. Chem.*, 2020, **2020**, 3644-3653.
139. E. J. Gao, B. Meng, J. Q. Su, T. T. Peng, Z. Z. Qi, B. Jia, Y. H. Feng and M. C. Zhu, *J. Struct. Chem.*, 2017, **58**, 1560-1566.
140. C. Liu, Y. Ouyang, B. Jia, Z. Zhu, J. Shi and H. Chen, *J. Mass Spectrom.*, 2012, **47**, 769-777.
141. J. W. Shin, *Int. J. Quant. Chem.*, 2021, **121**, e26532.
142. M. B. Burt, S. G. A. Decker and T. D. Fridgen, *Phys. Chem. Chem. Phys.*, 2012, **14**, 15118-15126.
143. L. Banu, V. Blagojevic and D. K. Bohme, *Int. J. Mass. Spectrom.*, 2012, **316**, 23-30.
144. C. G. Atkins, L. Banu, M. Rowsell, V. Blagojevic, D. K. Bohme and T. D. Fridgen, *J. Phys. Chem. B*, 2009, **113**, 14457-14464.
145. L. Banu, V. Blagojevic and D. K. Bohme, *Int. J. Mass. Spectrom.*, 2012, **330**, 168-173.
146. M. B. Burt and T. D. Fridgen, *J. Phys. Chem. A*, 2013, **117**, 1283-1290.
147. M.-L. Hu, A. Morsali and L. Aboutorabi, *Coord. Chem. Rev.*, 2011, **255**, 2821-2859.
148. S. Guillaumont, J. Tortajada, J.-Y. Salpin and A. M. Lamsabhi, *Int. J. Mass. Spectrom.*, 2005, **243**, 279-293.
149. C. Trujillo, A. M. Lamsabhi, O. Mo, M. Yanez and J.-Y. Salpin, *Int. J. Mass. Spectrom.*, 2011, **306**, 27-36.
150. J.-Y. Salpin, S. Guillaumont, J. Tortajada and A. M. Lamsabhi, *J. Am. Soc. Mass Spectrom.*, 2009, **20**, 359-369.
151. J.-Y. Salpin, V. Haldys, S. Guillaumont, J. Tortajada, M. Hurtado and A. M. lamsabhi, *ChemPhysChem* 2014, **15**, 2959-2971.
152. B. Power, V. Haldys, J.-Y. Salpin and T. D. Fridgen, *Int. J. Mass. Spectrom.*, 2018, **429**, 56-65.
153. O. Ali, N. M. Randell and T. D. Fridgen, *ChemPhysChem*, 2012, **13**, 1507-1513.
154. J.-Y. Salpin, S. Guillaumont, D. Ortiz, J. Tortajada and P. Maitre, *Inorg. Chem.*, 2011, **50**, 7769-7778.
155. J. Y. Salpin, L. Gamiette, J. Tortajada, T. Besson and P. Maitre, *Int. J. Mass Spectrom.*, 2011, **304**, 154-164.
156. J.-Y. Salpin, L. MacAleese, F. Chirot and P. Dugourd, *Phys. Chem. Chem. Phys.*, 2014, **16**, 14127-14138.

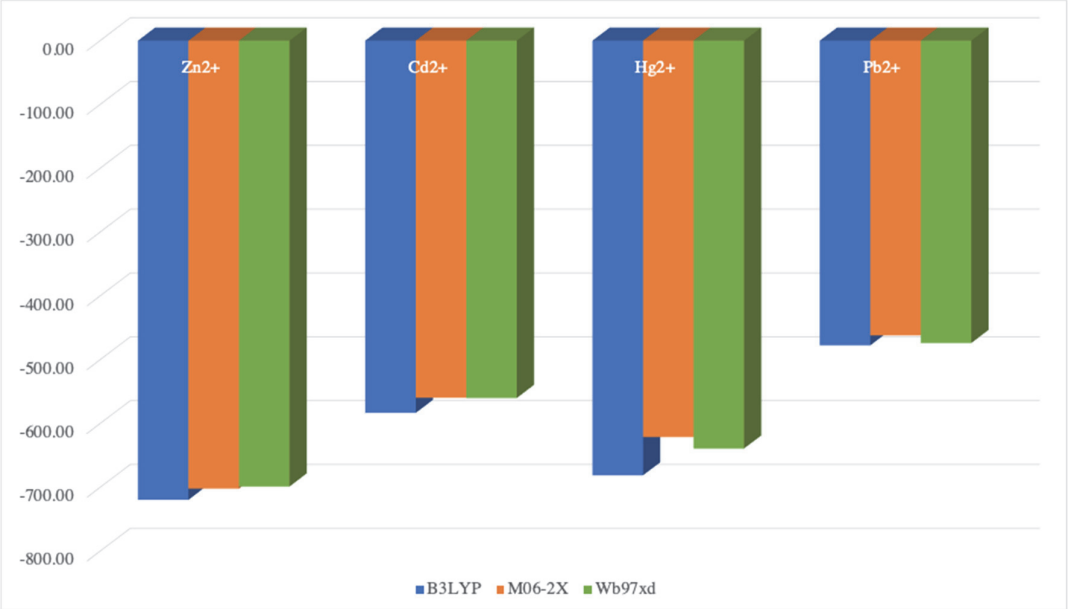

Figure S1. Comparison of the calculated binding energies (kJ·mol^{-1}) for urea-M^{2+} (M = Zn, Cd, Hg, Pb) complexes obtained with three different density functional theory methods, namely, B3LYP, M06-2X and ω-B97XD.

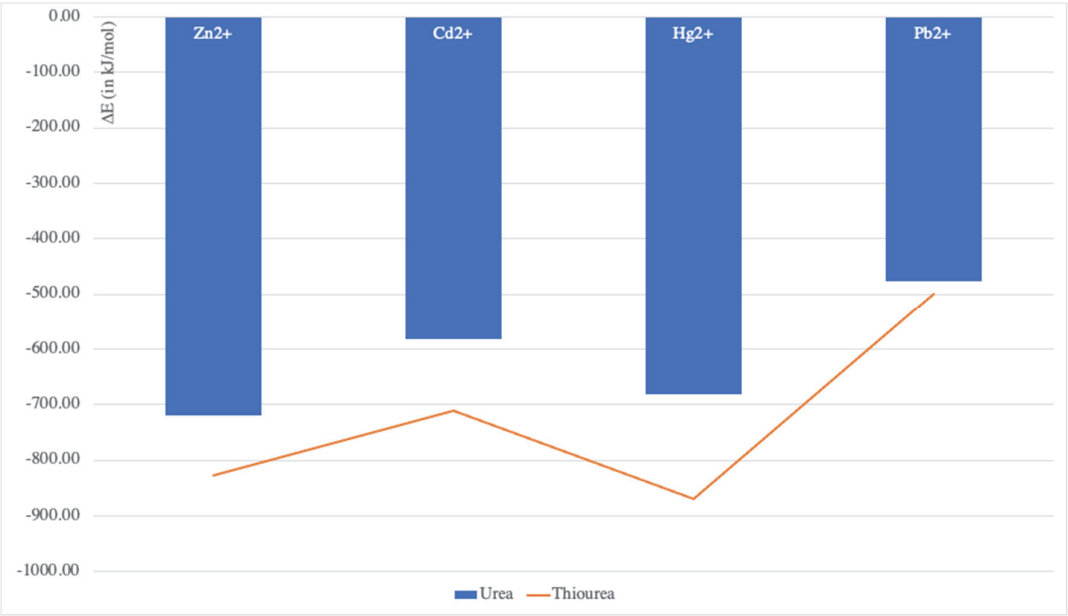

Figure S2. Variation of the calculated binding energies (kJ·mol^{-1}) for urea-M^{2+} (blue histogram) and thiourea-M^{2+} (orange line) (M = Zn, Cd, Hg, Pb) complexes.

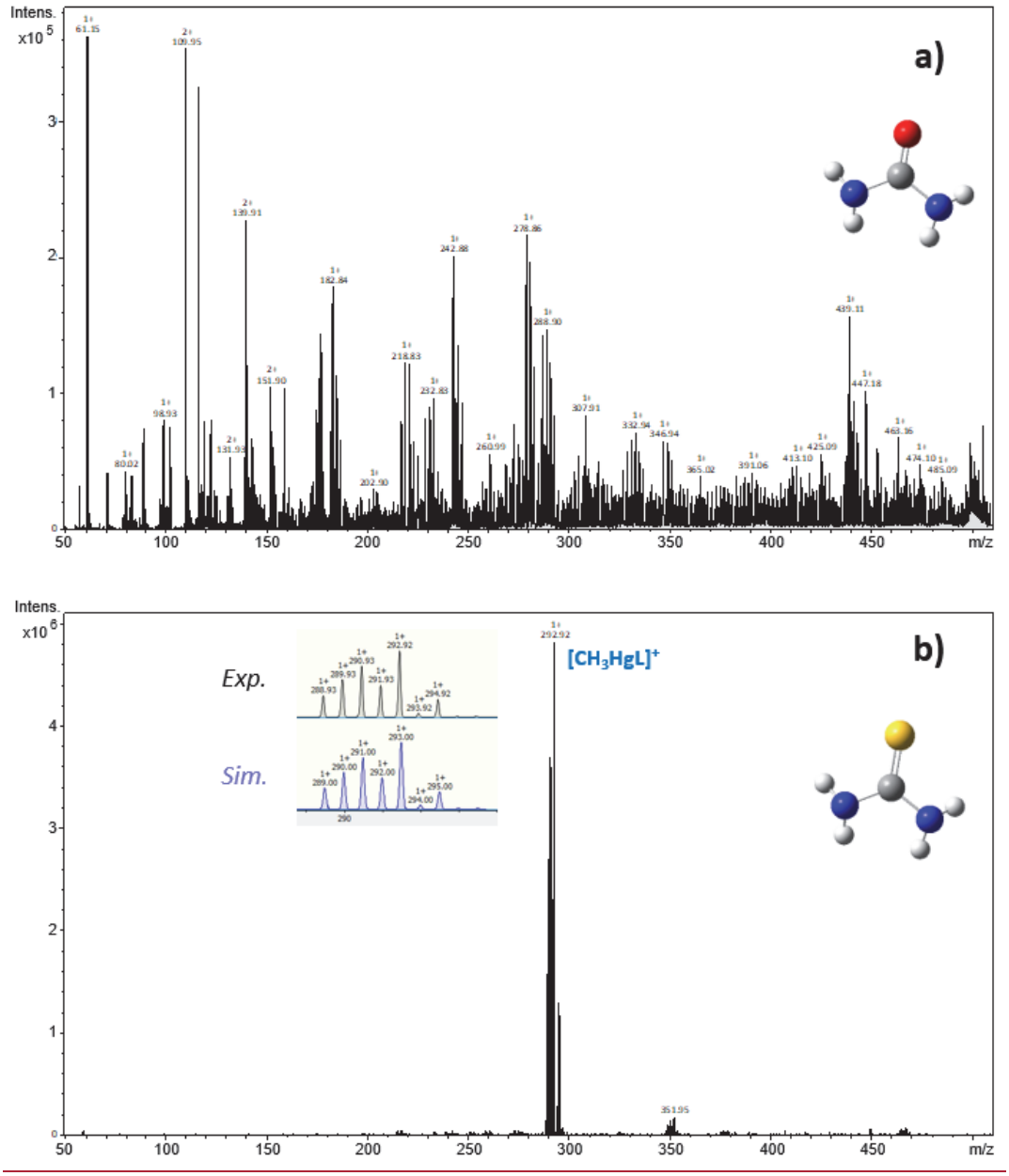

Figure S3. Positive-ion electrospray spectrum of an equimolar solution of CH_3HgCl and ligand L (10^{-4}M) in a water/methanol mixture (50/50 v/v) with **a)** L=urea and **b)** L=thiourea.
Mass spectra recorded on a Bruker Amazon speed ETD ion trap (capillary voltage: -4500V; dry gas: 4 L/min; nebulizer gas: 7.25 psi; dry temp: 180 °C; Cap Exit: 140 V ; Trap Drive 43.5; End plate offset: -500V; flow rate: 3 µl/min)

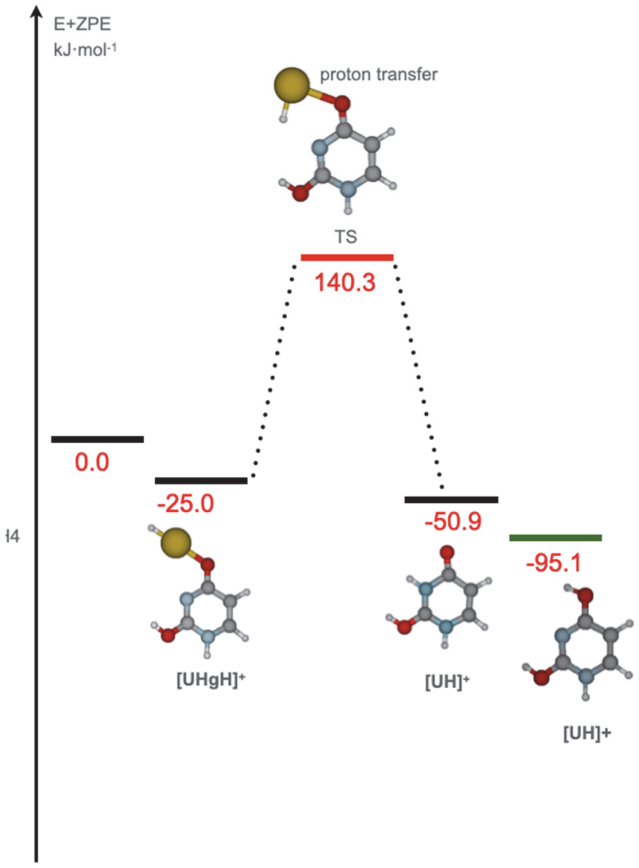

Figure S4. Proton transfer reaction from [UHgH$^+$] resulting from the beta-hydride elimination (Figure 3) to give protonated uracil. Relative energies plus zero-point energy (kJ·mol^{-1}) are shown in red color.

Table S1. Isomers of ethyl uracil cations [UEt]$^+$ at the B3LYP/6-31++G(d,p) level of theory. Energies are shown in kJ·mol^{-1}.

Keto forms	**E + ZPE**	**H**	**H rel**
U1	-493.62048	-493.61020	165.7
U2c	-493.65544	-493.64503	74.3
U2d	-493.65320	-493.64274	80.3
U3	-493.62583	-493.61542	152.0
U4a	-493.66781	-493.65756	41.4

U4b	-493.66508	-493.65484	48.6
U5	-493.64098	-493.63061	112.2
U6	Converged to U5		112.2
Enol forms			
E_U1a	-493.66996	-493.65990	35.2
E_U1b	-493.66523	-493.65508	47.9
E_U1c	-493.65192	-493.64160	83.3
E_U1d	-493.65035	-493.64001	87.5
E_U3a	-493.67016	-493.66009	34.8
E_U3b	-493.66628	-493.65616	45.1
E_U3c	-493.65657	-493.64623	71.1
E_U3d	-493.65343	-493.64297	79.7
E_U6a	-493.68236	-493.67210	3.2
E_U6b	-493.67798	-493.66763	15.0
E_U6c	-493.66555	-493.65507	47.9
E_U6d	-493.66323	-493.65268	54.2
E_U4ac	-493.66041	-493.65025	60.6
E_U4bc	-493.66685	-493.65668	43.7
E_U4ad	-493.64589	-493.63548	99.4
E_U4bd	-493.65426	-493.64388	77.3
E_U2ac	-493.66103	-493.65080	59.1
E_U2bc	-493.66773	-493.65756	41.4
E_U2ad	-493.64822	-493.63797	92.8
E_U2bd	-493.65689	-493.64671	69.9
Dienol forms			
dE_U1ac	-493.66410	-493.65416	50.3
dE_U1ad	-493.64880	-493.63865	91.0
dE_U1bc	-493.67059	-493.66069	33.2
dE_U1bd	-493.65721	-493.64714	68.8
dE_U3ac	-493.64445	-493.63421	102.7
dE_U3ad	-493.66009	-493.65008	61.0
dE_U3bc	-493.63512	-493.62457	128.0
dE_U3bd	-493.65333	-493.64318	79.1

dE_U6ac	-493.67651	-493.66637	18.3
dE_U6ad	-493.66169	-493.65130	57.8
dE_U6bc	-493.68343	-493.67333	**0.0**
dE_U6bd	-493.67039	-493.66007	34.8
dE'_U6ac	-493.65814	-493.64768	67.3
dE'_U6ad	-493.67228	-493.66209	29.5
dE'_U6bc	-493.65006	-493.63926	89.4
dE'_U6bd	-493.66584	-493.65548	46.9

Table S2. Isomers of ethylmercury uracil cations $[EtHg(U)]^+$ at the B3LYP/6-31++G(d,p)/DEF2-TZVPP level of theory. Energies are shown in $kJ \cdot mol^{-1}$.

Keto forms	**E + ZPE**	**H**	**H rel**
U1	-647.18844	-647.17502	116.3
U2c	-647.22409	-647.21080	22.3
U2d	-647.22179	-647.20840	28.6
U3	-647.19544	-647.18200	97.9
U4a	-647.23241	-647.21930	0.0
U4b	-647.22998	-647.21773	4.1
U5	-647.20184	-647.18850	80.9
U6	Converged to U5		80.9
Enol forms			
E_U1a	-647.22220	-647.20911	26.7
E_U1b	-647.21730	-647.20410	39.9
E_U1c	-647.20703	-647.19461	64.8
E_U1d	-647.20232	-647.18982	77.4
E_U3a	-647.22661	-647.21350	15.2
E_U3b	-647.22257	-647.20941	26.0
E_U3c	-647.21400	-647.20066	48.9
E_U3d	-647.21040	-647.19783	56.4
E_U6a	-647.19929	-647.18718	84.3
E_U6b	-647.19467	-647.18245	96.7
E_U6c	-647.18204	-647.16872	132.8

E_U6d	-647.17986	-647.16742	136.2
E_U4ac	-647.21854	-647.20549	36.3
E_U4bc	-647.22705	-647.21409	13.7
E_U4ad	-647.20378	-647.19042	75.8
E_U4bd	-647.21558	-647.20236	44.5
E_U2ac	-647.22585	-647.21288	16.9
E_U2bc	-647.23153	-647.21862	1.8
E_U2ad	Conv. to E_U2ac		16.9
E_U2bd	Not converged		-
Dienol forms			
dE_U1ac	-647.21670	-647.20370	41.0
dE_U1ad	-647.19777	-647.18629	86.7
dE_U1bc	-647.22322	-647.21027	23.7
dE_U1bd	-647.20629	-647.19396	66.5
dE_U3ac	-647.19995	-647.18753	83.4
dE_U3ad	-647.21755	-647.20542	36.4
dE_U3bc	-647.18631	-647.17426	118.3
dE_U3bd	-647.20879	-647.19649	59.9
dE_U6ac	-647.19330	-647.18128	99.8
dE_U6ad	-647.17857	-647.16630	139.2
dE_U6bc	-647.20003	-647.18805	82.1
dE_U6bd	-647.18708	-647.17395	119.1
dE_U6ac	-647.16874	-647.15638	165.2
dE_U6ad	-647.18305	-647.17095	126.9
dE_U6bc	Not converged		-
dE_U6bd	-647.17642	-647.16414	144.8